NASA/TM—1998-208658

Determination of Yield in Inconel 718 for Axial-Torsional Loading at Temperatures up to 649 °C

Christopher M. Gil and Cliff J. Lissenden
Pennsylvania State University, University Park, Pennsylvania

Bradley A. Lerch
Lewis Research Center, Cleveland, Ohio

November 1998

The NASA STI Program Office . . . in Profile

Since its founding, NASA has been dedicated to the advancement of aeronautics and space science. The NASA Scientific and Technical Information (STI) Program Office plays a key part in helping NASA maintain this important role.

The NASA STI Program Office is operated by Langley Research Center, the Lead Center for NASA's scientific and technical information. The NASA STI Program Office provides access to the NASA STI Database, the largest collection of aeronautical and space science STI in the world. The Program Office is also NASA's institutional mechanism for disseminating the results of its research and development activities. These results are published by NASA in the NASA STI Report Series, which includes the following report types:

- TECHNICAL PUBLICATION. Reports of completed research or a major significant phase of research that present the results of NASA programs and include extensive data or theoretical analysis. Includes compilations of significant scientific and technical data and information deemed to be of continuing reference value. NASA's counterpart of peer-reviewed formal professional papers but has less stringent limitations on manuscript length and extent of graphic presentations.

- TECHNICAL MEMORANDUM. Scientific and technical findings that are preliminary or of specialized interest, e.g., quick release reports, working papers, and bibliographies that contain minimal annotation. Does not contain extensive analysis.

- CONTRACTOR REPORT. Scientific and technical findings by NASA-sponsored contractors and grantees.

- CONFERENCE PUBLICATION. Collected papers from scientific and technical conferences, symposia, seminars, or other meetings sponsored or cosponsored by NASA.

- SPECIAL PUBLICATION. Scientific, technical, or historical information from NASA programs, projects, and missions, often concerned with subjects having substantial public interest.

- TECHNICAL TRANSLATION. English-language translations of foreign scientific and technical material pertinent to NASA's mission.

Specialized services that complement the STI Program Office's diverse offerings include creating custom thesauri, building customized data bases, organizing and publishing research results . . . even providing videos.

For more information about the NASA STI Program Office, see the following:

- Access the NASA STI Program Home Page at ***http://www.sti.nasa.gov***

- E-mail your question via the Internet to help@sti.nasa.gov

- Fax your question to the NASA Access Help Desk at (301) 621-0134

- Telephone the NASA Access Help Desk at (301) 621-0390

- Write to:
  NASA Access Help Desk
  NASA Center for AeroSpace Information
  7121 Standard Drive
  Hanover, MD 21076

NASA/TM—1998-208658

Determination of Yield in Inconel 718 for Axial-Torsional Loading at Temperatures up to 649 °C

Christopher M. Gil and Cliff J. Lissenden
Pennsylvania State University, University Park, Pennsylvania

Bradley A. Lerch
Lewis Research Center, Cleveland, Ohio

National Aeronautics and
Space Administration

Lewis Research Center

November 1998

Available from

NASA Center for Aerospace Information
7121 Standard Drive
Hanover, MD 21076
Price Code: A03

National Technical Information Service
5285 Port Royal Road
Springfield, VA 22100
Price Code: A03

DETERMINATION OF YIELD IN INCONEL 718 FOR AXIAL-TORSIONAL LOADING AT TEMPERATURES UP TO 649 °C

Christopher M. Gil and Cliff J. Lissenden
Pennsylvania State University
University Park, PA 16803

and

Bradley A. Lerch
National Aeronautics and Space Administration
Lewis Research Center
Cleveland, OH 44135

SUMMARY

An experimental program has been implemented to determine small offset yield loci under axial-torsional loading at elevated temperatures. The nickel-base superalloy Inconel 718 (IN718) was chosen for study due to its common use in aeropropulsion applications. Initial and subsequent yield loci were determined for solutioned IN718 at 23, 371, and 454 °C and for aged (precipitation hardened) IN718 at 23 and 649 °C. The shape of the initial yield loci for solutioned and aged IN718 agreed well with the von Mises prediction. However, in general, the centers of initial yield loci were eccentric to the origin due to a strength-differential (S-D) effect that increased with temperature. Subsequent yield loci exhibited anisotropic hardening in the form of translation and distortion of the locus.

This work shows that it is possible to determine yield surfaces for metallic materials at temperatures up to at least 649 °C using multiple probes of a single specimen. The experimental data is first-of-its-kind for a superalloy at these very high temperatures and will facilitate a better understanding of multiaxial material response, eventually leading to improved design tools for engine designers.

INTRODUCTION

Aeropropulsion components, such as disks, blades, and shafts are commonly subjected to multiaxial stress states at elevated temperatures. Nickel-base alloys are often used for these applications because of their excellent elevated temperature mechanical properties. Experimental results from loadings as complex as those felt in-service are needed to help guide the development of accurate viscoplastic multiaxial deformation models that can be used to improve the design of aeropropulsion components.

Inconel 718 (IN718) is a popular nickel-base alloy which has been extensively researched in terms of strengthening mechanisms and fatigue behavior (e.g., Oblak, et al., 1974; Fournier and Pineau, 1977; Sundararaman et al., 1988; Worthem et al., 1989; Kalluri et al., 1997). In addition, the viscoplastic behavior of IN718 at 649 °C has been characterized for the Chaboche and Bodner-Partom viscoplasticity models using tensile loading at several strain rates (Abdel-Kader et al., 1986; Li, 1995). In this investigation, tubular IN718 specimens were subjected to isothermal combined loads over a wide range of temperatures (23 to 649 °C) to map out yield loci in the axial-shear stress plane. The results over this broad temperature range are unique and will lead to a better understanding of time-dependent multiaxial behavior of IN718 in service at elevated temperatures.

Multiaxial experimental investigations often use a yield surface to delimit the elastic region, describe hardening, and determine if an associated flow rule applies by checking for normality (Michno and Findley, 1974; Phillips and Moon, 1977; Khan and Wang, 1993). These experiments involve determining enough yield points in one or more stress planes to construct the yield surface. This can be accomplished using several specimens, where each specimen is used to find a single yield point, or by using a single specimen to determine multiple yield points. The latter technique is more common since using several specimens is not cost efficient and the results may be affected by specimen-to-specimen scatter. For an in-depth (albiet dated) literature review of multiaxial experimental investigations, see Hecker (1976) and Michno and Findley (1976).

The success of using a single specimen to completely map out a yield surface depends strongly on preserving the material state during probing. Since yielding defines the onset of plastic deformation, any change in material state associated with detecting a yield point must be insignificant. Otherwise, the material state (and along with it the size and shape of the yield surface) is changed by each probe.

Historically, three types of yield definitions have been used for yield surface experiments: (1) deviation from linearity, (2) offset strain, and (3) back-extrapolation. The *small offset strain* definition is frequently used to give an indication of the proportional limit. As the name implies, yielding is defined to occur when an equivalent offset strain on the order of a few microstrain (με) has developed.

There is some flexibility in using the small offset definition of yielding since there are a wide range of offset magnitudes that can be considered small. Helling et al. (1986) detected offset strains of ~5 με to determine yield surfaces for aluminum and brass, whereas at the other extreme Nouailhas and Cailletaud (1996) used a target value of 100 με when conducting similar tests on a single-crystal superalloy. For elevated temperature experiments, where 'heater noise' (thermal fluctuations and electronic noise) can decrease the strain signal-to-noise ratio, a large enough offset strain must be used to determine yield points consistently. Thus, in the present work we investigated the effect of using target values between 10 and 30 με for determining the yield points.

The accuracy of the experimental results is strongly dependent on the strain measurement device. High precision strain gages work well for detecting small increments of strain at room temperature (Helling et al., 1986; Wu and Yeh, 1991). However, for high test temperatures, where strain gages cannot be readily used, a different method must be applied to detect yielding, such as an acoustic emission system (Winstone, 1983) or a high temperature biaxial extensometer (Battiste and Ball, 1986; Lissenden et al., 1997).

In the present study, a biaxial extensometer was used to determine yield loci in the axial-shear stress plane for tubular IN718 specimens over a wide range of temperatures (23 to 649 °C). The specimens were tested in two distinct material states: solutioned and aged. The aged material contains precipitates that are expected to hinder dislocation movement and may lead to large back stresses (Stouffer and Dame, 1996), while the solutioned material is generally a single-phase composition. Clearly, the two materials will exhibit different yielding and hardening behavior.

The objective of this study was to demonstrate that yield loci (initial and subsequent) can be determined for metallic materials (such as IN718) at temperatures up to 649 °C by probing a single specimen multiple times and measuring strains with a biaxial extensometer. This work opens the door for a more in-depth study of multiaxial response at temperatures in the service range of aeropropulsion systems. The data presented here will be further analyzed in a companion paper (Gil et al., 1998a) to obtain loci of rate-dependent flow surfaces in the axial-shear stress plane.

EXPERIMENTAL SETUP AND PROCEDURE

Material and Specimens

The wrought Inconel 718 superalloy used in this study was obtained in the form of extruded 31.8 mm diameter bar stock, all from the same heat. The material composition as provided by the fabricator is listed in Table I. The bars were machined into tubular specimens having the final dimensions shown in figure 1. After machining, the specimens were solutioned at 1038 °C in argon for 1 hr and air cooled. Select specimens were further heat-treated as follows: aged at 720 °C in argon for 8 hr, cooled at 55 °C/hr to 620 °C and held for 8 hr, then air cooled to room temperature. Henceforth, the material state will be referred to as either *solutioned* or *aged*.

Metallography was performed on transverse and longitudinal sections taken from the grip ends (undeformed) and from the gage sections (deformed) of both solutioned and aged tubes. No difference was observed between the grip and the gage sections. Furthermore, both the solutioned and aged microstructures appeared similar (fig. 2). The grain structure consisted of equiaxed grains having an ASTM grain size of 4 (a nominal diameter of 90 μm). The solutioned material had a hardness of HRB 90, while the aged material was HRC 45. Carbide stringers were aligned parallel to the tube axis (i.e., the extrusion axis) and were observed distributed throughout the microstructure.

Transmission electron microscopy was performed on the solutioned and aged IN718. The aged material was observed to have a fine dispersion of γ" within each grain (fig. 3). The precipitate particles were observed to be platelets ~10 to 15 nm in length. The solutioned IN718 did not show any precipitation. Texture analysis was also performed, which showed there to be no preferred grain orientation for either heat treatment.

Test Equipment

The experiments were performed on a computer controlled biaxial servohydraulic test machine capable of applying an axial load of ±222,000 N and a twisting moment of ±2,260 N·m. The specimen was held in place by water-cooled, hydraulically actuated grips. The top grip remained fixed throughout a test while the bottom grip is attached to an actuator capable of independent rotation and vertical translation. An analog controller was used to command the motion of the actuator. Additional details regarding the biaxial test machine are provided by Kalluri and Bonacuse (1990).

The test machine is equipped with a closed-loop induction heating system (Ellis et al., 1997) capable of specimen temperatures in excess of 800 °C. The system consists of a 5-kW radio frequency induction heating unit and three adjustable, water-cooled copper coils that surround the gage section of the specimen (fig. 4). The specimen temperature is controlled by spot welding a thermocouple to the gage section of the specimen. Three additional thermocouples were spot welded to the specimen to help achieve an acceptable thermal gradient (±1 percent of the test temperature).

Strain Measurement

The ability to measure very small increments of strain (precise to the microstrain level) is necessary for yield surface experiments, since the goal is to detect yielding and then unload the specimen before significant permanent deformation occurs. Furthermore, the strain measurement device must maintain this level of performance for a wide range of specimen temperatures. This is especially difficult at elevated temperatures, where thermal fluctuations can hinder high resolution strain measurement.

In this investigation, axial and shear strains were measured using a water-cooled biaxial extensometer (fig. 4) that is capable of operating over a large temperature range. The extensometer uses two high-purity alumina (Al_2O_3) rods, spaced 25 mm apart, to precisely measure axial deformation and twist. Strain values are recorded to one tenth of a microstrain (με). Lissenden et al. (1997) have supplied more details on the biaxial extensometer.

For transverse strain measurement, a diametral extensometer was employed. The diametral extensometer is similar to the biaxial extensometer in appearance, although it contains longer rods that rest on either side of the gage section of the specimen to directly measure the change in diameter. Transverse strains were measured to determine Poisson's ratio (which will be used to calculate the equivalent strain rate) and to determine whether Poisson's ratio changes during the course of a yield locus probe.

Test Control

With one exception, all of the experiments were conducted in strain control. An equivalent strain rate of 10 με/sec (10^{-5} s^{-1}) was used. For axial-torsional loading and a Poisson's ratio of 0.34,[1] the equivalent strain rate is

$$\dot{\varepsilon}_{eq} = \sqrt{\frac{2}{3}\dot{\varepsilon}_{ij}\dot{\varepsilon}_{ij}} = \sqrt{(0.906)^2\dot{\varepsilon}_{11}^2 + \frac{4}{3}\dot{\varepsilon}_{12}^2} \tag{1}$$

where $\dot{\varepsilon}_{ij}$ is the strain rate tensor and $\dot{\varepsilon}_{11}$ and $\dot{\varepsilon}_{12}$ denote the axial and shear strain rates, respectively.

Custom written software and a personal computer, equipped with analog-to-digital (A/D) and digital-to-analog (D/A) conversion hardware, were used to control the experiments. The D/A hardware was commanded to send strain increment data to the electronic controller 1000 times/sec. Similarly, the A/D hardware collected load, torque, and strain data from the controller at 1000 Hz. Every 100 data points were averaged to help minimize the effect of heater noise, which resulted in a maximum of 10 data points per second being written to a file.

Two different software programs were developed for controlling the experiments. One program was used to determine the individual yield points that were used to map out initial and subsequent yield loci and the other program performed the radial prestrains.

[1]Measured at 23 °C. Abdel-Kader et al. (1986) obtained a value of 0.3356 at 649 °C.

Yield Loci

Each locus was determined by straining the specimen in 16 unique directions, according to a specified angle in equivalent axial-torsional strain space (fig. 5). The order in which the probes were conducted was chosen to minimize changes to the material state. For example, figure 5 shows that each even-numbered probe was in the opposite direction from the preceding odd-numbered probe. By using this sequence we hoped to counter balance the effects of the previous probe. Furthermore, each surface was repeated at least once to ensure that the results were repeatable and to verify that the material state remained essentially undisturbed.

Each point on the yield locus was determined using the following procedure.

- Calculate the coefficients of the axial and shear elastic loading lines (E, σ_{11}^{o}, G, and σ_{12}^{o}) over a predefined strain range during the initial (assumed to be linear elastic) portion of the loading using a least squares regression technique (fig. 6). E and G are the axial and shear moduli; σ_{11}^{o} and σ_{12}^{o} are the axial and shear initial stresses.
- Continually calculate the offset strain components (fig. 6)

$$\varepsilon_{11}^{off} = \varepsilon_{11} - \frac{\sigma_{11} - \sigma_{11}^{o}}{E} \tag{2}$$

$$\varepsilon_{12}^{off} = \varepsilon_{12} - \frac{\sigma_{12} - \sigma_{12}^{o}}{2G} \tag{3}$$

  where σ_{11}, σ_{12} are the axial and shear stresses and ε_{11}, ε_{12} are the axial strain and tensorial shear strain ($\varepsilon_{12} = 1/2\ \gamma_{12}$).
- When the equivalent offset strain,

$$\varepsilon_{eq}^{off} = \sqrt{\frac{2\left(1+2\nu^{2}\right)}{3}\left(\varepsilon_{11}^{off}\right)^{2} + \frac{4}{3}\left(\varepsilon_{12}^{off}\right)^{2}} = \sqrt{\left(\varepsilon_{11}^{off}\right)^{2} + \frac{4}{3}\left(\varepsilon_{12}^{off}\right)^{2}}, \tag{4}$$

  reaches the target value (usually 30 με), write the current stress values (axial and shear) to an output file, unload the specimen and then begin the next probe.

Equation 4 is the equivalent offset strain, simplified for axial-torsional loading of a material exhibiting inelastic incompressibility ($\nu = 0.5$). Although the incompressibility condition may not be met for small offset strains, where the instantaneous Poisson's ratio is transitioning from its elastic value to its fully inelastic value, this relationship for the offset strain components has been traditionally used by researchers for determining yield surfaces (e.g., Wu and Yeh, 1991; Khan and Wang, 1993; Lissenden, et al., 1997). Additionally, the equivalent offset strain refers to an offset during loading and does not necessarily have the same magnitude as the permanent set (i.e., permanent strain at zero load).

Radial Prestraining

After determining the initial yield loci, hardening behavior was studied by applying radial prestrains at elevated temperature (except in one case a cyclic radial prestrain was applied at room temperature). Two radial prestrain paths were used. One path was combined tension-torsion, corresponding to an angle of ∠45° in the equivalent strain plane (fig. 7(a)). This was equivalent to a ∠45° path in the equivalent stress plane. A schematic of the equivalent stress-strain response is shown in figure 7(b). The maximum prestrain point was determined by detecting a particular value of equivalent offset strain. The other prestrain path consisted of straining the specimen in pure tension until a predefined total axial strain was achieved.

The same procedure was followed for both strain paths and is outlined in the following:

- The stress-free specimen was heated to the desired temperature (in load and torque control).
- After thermal equilibrium was reached, the specimen was strained until the target prestrain value was achieved (point A_1 (or B_1) in fig. 7(a)).
- The mode was switched to load/torque control and the specimen was held at a constant stress for several minutes. During this time creep strains were monitored on X-Y plotters and recorded by the data acquisition software.

- After several minutes, the control mode was switched back to strain control. The reverse yield point was found (point A_2 (or B_2) in fig. 7(a)) by unloading the specimen until the equivalent offset strain exceeded the target value.
- The specimen was reloaded to a point (point A_3 (or B_3) in fig. 7(a)) midway between the prestrain point and the reverse point. The subsequent yield locus was then determined using this point as the probe origin.

EXPERIMENTAL RESULTS

Solutioned IN718

When using the offset strain definition of yielding it is important to relate the offset strain during loading to the permanent set that is measured after unloading is complete. In an attempt to compare these two quantities, the offset strain for a small offset tension test was plotted versus the total axial strain (fig. 8). The offset strain accumulates to ~30 με during loading, however the offset strain continues to increase during unloading to a total offset of ~44 με.

The discrepancy between the offset strain during loading and the permanent set is believed to be due to inaccuracy of the extensometer after a load reversal, rather than true material behavior. Data from previous tests on type 316 stainless steel (Lissenden et al., 1997) were analyzed, where an extensometer and strain gages were both used to measure strain. A comparison of strain data obtained from the extensometer and from the strain gages showed that there was good agreement between the two measurement devices during loading. However, after the load reversal the extensometer offset strains often continued to increase while the strain gages indicated linear elastic unloading (constant offset strain). This suggests that strains measured by the extensometer during loading are accurate, but that a correlation between the offset strain and permanent set cannot be made.

Now that we were confident that the extensometer was accurately measuring the offset strain, specimen IN-15 was used to determine which control mode, stress or strain, gave more consistent results at 23 °C. Phillips et al. (1984) investigated the yield behavior of aluminum using stress and strain controlled loading, however a direct comparison of the results was not shown. In this preliminary work we were interested in comparing the size and shape of the yield locus using stress and strain control and we wanted to determine if there was more or less scatter in the results for strain control compared to stress control.

Initial yield loci for specimen IN-15 were determined under stress and strain controlled loading at room temperature. In these tests the target value was an equivalent offset strain of 20 με. The resulting loci are plotted in the modified normal-shear stress plane ($\sqrt{3}\cdot\sigma_{12} - \sigma_{11}$) in figure 9. The eccentricity of the locus in the compression direction may or may not be significant, since specimen IN-15 was not in the pristine state prior to these tests. Clearly, the control mode had little effect on the data. Repetitive tests were made to verify this result. Strain control was used for the remaining experiments to be consistent with prestraining.

Next, the elastic Poisson's ratio (which was needed for eq. (1)) was determined during a tensile probe by measuring the diametral strain. Specimen IN-9 (a pristine specimen) was tested in tension until a 10 με offset was reached. Figure 10 shows the diametral strain (ε_{22}) plotted versus the axial strain (ε_{11}). The slope of figure 10, which is Poisson's ratio, is 0.34 and remains constant up to the load reversal. This suggests that the elastic Poisson ratio (0.34) is a more appropriate choice for use in equation (4) when performing small offset yield experiments since no significant change in the Poisson ratio occurs. However, results not shown here indicate that yield loci are relatively insensitive to the Poisson ratio for values ranging between 0.25 and 0.5 (Gil, 1998).

The effect of using target values between 10 and 30 με to determine yield loci was examined next. Three loci were determined for each target value to judge repeatability. At each target value, the results of the three loci were nearly identical (Gil, 1998); indicating that target values in this range do not significantly change the material state. Additionally, no significant hardening occurred in the offset strain range of 10 to 30 με. We chose to use a target value of 30 με for the remaining experiments to obtain a maximum amount of offset strain data to analyze in terms of rate-dependent flow definitions; which for viscoplastic materials are more important than the yield definition (Gil et al., 1998a). Here, a rate-dependent flow definition refers to one that depends on the inelastic strain rate, rather than the total inelastic strain. Additionally, at elevated temperatures thermal fluctuations decrease the resolution of the measured strain, making a larger target value more practical.

After these preliminary issues were resolved, the initial yield behavior of solutioned IN718 was investigated at 23 °C using two pristine specimens (IN-6 and IN-25). There was remarkably very little specimen-to-specimen scatter between the initial loci (fig. 11). Furthermore, each test was repeated once to confirm that no significant change in material state took place during probing.

The von Mises and Tresca yield criteria (see, for example, Khan and Huang, 1995) are the two most popular criteria for predicting yielding in isotropic metals. The von Mises criterion plots as a circle in the modified axial-shear stress plane ($\sqrt{3}\cdot\sigma_{12} - \sigma_{11}$), while the Tresca criterion plots as an ellipse. These criteria are compared with the experimental data in figure 11. The von Mises circle, centered at the stress plane origin with a radius of 248 MPa, appears to fit the data well. The Tresca ellipse provides a more conservative prediction of yielding when torsional loads are present.

Before investigating the initial yield behavior at elevated temperature the heater noise in the strain signals at elevated temperature was evaluated through comparison with room temperature measurements (fig. 12). The peak-to-peak amplitude of the electronic noise was well below 1 με for both axial and shear strain at room temperature. At elevated temperature (454 °C), the amplitude is larger (especially in the axial strain) due to small thermal fluctuations and electronic noise associated with the induction heating system. Clearly, heater noise is important when attempting to measure strains precise to a few microstrain. After a great deal of effort to further reduce the heater noise without success, it was viewed as acceptable.

Initial yield loci for specimens IN-6 and IN-25 determined at 371 and 454 °C are shown in figures 13 and 14, respectively. Solutioned IN718 was not tested at 649 °C because that is felt to be too close to the aging temperature. As the temperature increases, the yield loci decrease in size, but retain the same shape. In addition, the center of the locus is not located at the origin of the stress plane as it was at 23 °C. A von Mises circle with a radius of 207 MPa centered at (–13.8, 0.0) MPa in the modified axial-shear stress plane appears to fit the data at 371 °C very well (fig. 13). At 454 °C (fig. 14), a von Mises circle with a radius of 193 MPa and centered at (–27.5, 0.0) was fit to the data by eye. These results indicate that as the temperature increases, the yield locus decreases in size and becomes more eccentric to the origin. The eccentricity in the compression direction will be discussed later in conjunction with the aged IN718.

Next, specimen IN-6 was subjected to combined axial-torsional prestraining, as shown in figure 15. Point A corresponds to the location where the initial loci were determined (zero stress). Subsequent yield loci were determined at locations C, O, Q, and S.

The first prestrain consisted of combined tension-torque loading at 454 °C. Specimen IN-6 was strained along a ∠45° radial path in equivalent strain space (path $OA_1A_2A_3$ in fig. 7(a)) until an equivalent offset strain of 500 με was attained (which corresponded to a stress state of σ_{11} = 173.5 MPa, σ_{12} = 92.0 MPa; point B in fig. 15). The center of the elastic region (point C) was then found, as described in the previous section, and two subsequent loci were determined.

The first subsequent yield locus (Locus C) is shown in figure 16, along with the prestrain point B. A spline fit of the yield locus is included to aid in interpreting the data. There is clearly some translation of the yield locus toward the prestrain point. Furthermore, the back of the locus has become flattened indicating some distortional hardening. Various researchers have observed similar results for monolithic metals such as aluminum (Phillips et al., 1972), brass (Helling et al., 1986), and stainless steel (Wu and Yeh, 1991). Figure 16 also indicates that neither isotropic hardening (a pure expansion of the yield surface), nor kinematic hardening (a pure translation of the yield surface), nor a simple combination thereof accurately describe the hardening behavior of solutioned IN718 at 454 °C. Furthermore, the locus shows a small amount of cross effect, that is, an expansion of the locus in the directions perpendicular to the prestrain direction.

Solutioned IN718 exhibited very little hardening behavior during the first prestrain cycle at 454 °C. Upon reaching prestrain point B, the axial and shear responses were nearly perfectly plastic. In an attempt to determine the effect of fully reversed cyclic loading on material hardening, specimen IN-6 was subjected to five strain-controlled cycles of combined axial-torsional loading at 23 °C, beginning and ending at zero stress (figs. 15 and 17). The radial strain path was oriented at an angle of ∠45° for positive strains and ∠225° for negative strains (as measured counterclockwise from the positive axial strain axis) and had limits of $\varepsilon_{11} = \pm 2500$ με and $\varepsilon_{12} = \pm 1875$ με.

The last cycle ended when the axial and torsional loads reached zero, thus the final loading was in the ∠225° direction. Terminating the final cycle at zero stress (point O in fig. 17) led to an equivalent offset strain of 1625 με between points O and D. Specimen IN-6 was then reheated to 454 °C and a subsequent yield locus was determined. Figure 18 shows the subsequent locus (Locus O) as well as the cyclic prestrain path. As expected, the locus has been translated and distorted in the ∠225° direction compared to locus C and its center is located at approximately the same position as the initial Mises circle. It also appears that the cyclic loading may have slightly increased the yield strength in the directions perpendicular to the loading path (i.e., cross effect).

Specimen IN-6 was again prestrained in the ∠45° direction at 454 °C until an equivalent offset strain of 1000 με was achieved (which corresponded to a stress state of σ_{11} = 162.0 MPa, σ_{12} = 86.0 MPa; point P, fig. 15). Locus Q was then determined, as shown in figure 19, and was again translated in the direction of prestrain and distorted. From this point, specimen IN-6 was then further prestrained until an additional offset strain of 500 με was reached (corresponding to a stress state of σ_{11} = 177.0 MPa, σ_{12} = 100.0 MPa; point R, fig. 15), and locus S was determined (fig. 19). For each locus shown in figure 19, the corresponding prestrain point is shown to provide a reference. Loci Q and S are very similar in shape and size, however locus S is shifted slightly more in the prestrain direction with respect to locus Q due to the additional prestrain. Additionally, the loci exhibit a cross effect, that is they have expanded slightly in the direction perpendicular to the prestrain direction.

Aged IN718

Experiments to determine yield loci for aged IN718 were hindered by an anomalous material response, termed *stiffening* (Gil et al., 1998b), that occured during compressive loading. Stiffening is a nonlinear material response that is characterized by a slight increase in the stiffness. This behavior is shown in figure 20, where the offset strain initially has a positive sign for compressive loading. At some point, as indicated in figure 20, the direction of the offset strain reverses. Again during unloading, the offset strain continues to increase. As mentioned, the permanent set shown in figure 20 may not be representative of the true material behavior since the extensometer appears to exhibit hysteresis upon reversing the load. If the true material response were elastoplastic, then the permanent set should be 30 με, which would make the error in the extensometer results after complete unloading ~17 με (the maximum compressive strain was 3720 με).

Stiffening could be associated with nonlinear interactions between dislocations and precipitate particles. Hirth and Cohen (1970) proposed a theory to account for the strength-differential (S-D) effect in steels, in which dislocations interact with solute atoms causing local distortion of the lattice and leading to local elastic strains that are nonlinear. According to the model, the compressive nonlinear elastic region has an increasing instantaneous stiffness. Thus, the yield stress is higher than that of a material having a linear elastic region (given the same amount of elastic strain). Additionally, the tensile nonlinear elastic region has a decreasing instantaneous stiffness and therefore the yield stress is lower than that of a material having a linear elastic region. Kalish and Cohen (1969) suggest that this theory can also apply to the coherency strains around precipitated particles.

Stiffening presented a real challenge to our procedure for detecting yielding because our existing procedure explicitly assumes an initial linear elastic response. If stiffening is an elastic response (which appears to be the case), then inelastic strain begins to occur when the stiffening offset has reached a maximum (fig. 20). Therefore, in the presence of stiffening, we took the inelastic strain to be the offset strain plus the maximum stiffening strain. Doing so essentially shifts the elastic loading line in the direction of the stiffening.

Two pristine aged IN718 specimens (IN-8 and IN-10) were tested at 23 °C and the initial yield loci are shown in figure 21. The tests were repeated once for each specimen with nearly identical results. A von Mises circle of radius 655 MPa appears to fit the data well, that is 2.64 times larger than the initial von Mises circle for solutioned IN718 at 23 °C. Clearly, the aging process (precipitation) effectively strengthens the material. However, unlike the solutioned specimens (fig. 11) the locus is extremely eccentric to the stress origin and centered at (–138, 0) MPa. The eccentricity of the locus in the compression direction is representative of the S-D effect that has been observed in select materials (martensitic steels and other alloys as well as plastics). Hirth and Cohen (1970) and Drucker (1973) provide possible explanations for the S-D effect. The Hirth and Cohen explanation involves nonlinear elasticity and was mentioned previously. Drucker's explanation is based on the experimental observation that materials that exhibit a S-D effect also have a permanent volume change, which implies that yielding is dependent upon the mean stress $\left(\sigma_m = \left[\sigma_{11} + \sigma_{22} + \sigma_{33}\right]/3\right)$. Permanent volume change is generally related to an increased dislocation density required for inelasticity in dispersion hardened materials. If yielding is a linear function of mean stress, then there is a S-D effect. See also Radcliffe and Leslie (1969), Drucker (1973), Rauch et al. (1975), and Spitzig et al. (1975) for more on the strength-differential effect.

There appears to be more scatter in the aged IN718 results than for the solutioned IN718 results. This is probably due at least in part to the gradual yielding exhibited by the aged material relative to the solutioned IN718. Figure 22 shows the normalized von Mises effective stress, $\sigma_{eff} = \sqrt{3J_2}/\sigma_{PL}$ for equivalent offset strains up to 30 με for both materials under combined tension/torsion (θ = 57°) at 23 °C. Here, J_2 is the second invariant of deviatoric stress and σ_{PL} is the proportional limit. The smaller hardening modulus of the solutioned IN718 results in minimal scatter because of the smaller resulting stress increment relative to the aged IN718.

Specimens IN-8 and IN-10 were then tested at 649 °C (fig. 23). Following the same trend that was observed for solutioned IN718, the loci are similar in shape to the loci at 23 °C, yet smaller in size and translated further in the compression direction. A von Mises circle with a radius of 448 MPa and centered at (–145.0, 0.0) MPa appears to closely fit the data from both specimens. More scatter is observed at 649 °C due to the effect of heater noise. The yield loci for both solutioned and aged IN718 appear to translate in the compression direction with increasing test temperature, as indicated in table II. This means that the S-D effect, which is defined mathematically in the discussion section, increases with temperature, but Rauch et al. (1975) report that the S-D effect decreases with temperature for some steels. Additional initial yield surface determinations for aged IN718 at 371 and 454 °C (not reported herein) indicate that the temperature-dependence of yielding is different for IN718 in the aged state than it is in the solutioned state.

Specimen IN-10 was subjected to a combined axial-shear prestrain ($\angle 45°$ in equivalent strain space) at 649 °C until an equivalent offset of 500 με was detected. The subsequent yield locus is shown in figure 24, where the initial Mises circle is also shown for reference. During the prestrain procedure the center of the locus was not accurately located, possibly due to the influence of heater noise, which may have led to the scatter in the data points on the yield locus. Nevertheless, a few important characteristics can still be observed. First, the locus is translated further in the direction of the prestrain than was observed for solutioned IN718 (fig. 16). This verifies that precipitation hardening IN718 not only increases the yield strength of the material but also increases its ability to strain harden (Dieter, 1988). Additionally, there appears to be no cross effect, however it is difficult to make any strong conclusions based on the limited amount of data.

The other aged specimen (specimen IN-8) was subjected to a purely tensile prestrain until a total axial strain of 9000 με (0.9 percent) had been reached. The first subsequent yield locus is shown in figure 25. The locus translated in the direction of prestrain and distorted. The distortion is an elongation in the direction of the prestrain in addition to a flattening of the back side. No cross effect is observed.

DISCUSSION

All initial yield loci exhibit an S-D effect (except for solutioned IN718 at room temperature) for a 30 με offset strain yield definition. The S-D effect increases as the test temperature increases and for aged IN718 at 649 °C is 65 percent based on the definition of strength differential commonly used (Spitzig, et al., 1975),

$$SD = 2\frac{|\sigma_c| - |\sigma_t|}{|\sigma_c| + |\sigma_t|} \times 100\%, \tag{5}$$

where σ_c and σ_t are the yield strengths in compression and tension, respectively. Equation (5) was used to calculate the strength-differential shown in table II. When interpretting this definition based on the Mises yield locus in the modified stress plane shown in figure 23, *SD* is the percentage of the ratio of circle center to diameter. Whether the S-D effect that we have observed is *real* or *apparent* is currently being investigated. A *real* S-D effect remains during gross plastic deformation, while an *apparent* S-D effect is only present at the initiation of plastic deformation and could be due to residual stresses or microcracks among other things (see Hirth and Cohen, 1970 and Drucker, 1973). The real S-D effect in 4310 and 4330 steels was found to be 5.5 percent by Spitzig et al. (1975). We suspect that a large portion of the 65 percent S-D effect that we have observed is apparent rather than real. However, in order to mathematically predict our experimentally determined yield loci the S-D effect, real or apparent, must be taken into account. One way to do that is to use a Drucker-Prager (1952) type yield criterion, that is, one that depends on the first stress invariant, $I_1 = 3\sigma_m$, and thus depends on the mean stress. Alternatively, the third deviatoric stress invariant, J_3, could be used if yielding is independent of the mean stress.

The subsequent yield loci indicate that IN718 exhibits kinematic hardening, which results in a Bauschinger effect, as well as distortional hardening, which is commonly observed in yield surface experiments when a proportional limit or small offset strain definition is used. It is commonly observed that small offset strain definitions result in hardening that is primarily kinematic and distortional while large offset strain definitions (e.g., 2000 με) result in isotropic hardening (Williams and Svensson, 1971 and Khan and Wang, 1993). However, solutioned IN718 exhibited only a small amount of hardening relative to aged IN718.

Experimentally determined subsequent yield loci have two primary purposes. In one case, they can provide guidance for the development of evolution equations that are necessary for materials that exhibit hardening. In another case, they can be used to validate material models that have been developed and characterized from other, perhaps uniaxial, data. We view the limited subsequent yield loci presented herein as insufficient for

either of these purposes, but present it as a demonstration that this type of data can now be obtained and will undertake a detailed study of hardening behavior in the future.

SUMMARY AND CONCLUSIONS

The effort to determine initial and subsequent yield loci for IN718 at temperatures up to 649 °C has been successful. Yield loci were determined for solutioned IN718 at temperatures of 23, 371, and 454 °C and for aged (precipitation hardened) IN718 at temperatures of 23 and 649 °C. This work opens the door for more detailed studies on hardening behavior at high temperatures. The following general conclusions can be made based on the experimental results of this work.

- The von Mises yield criterion fit the initial yield loci in the axial-shear stress plane very well if an initial eccentricity is considered (see table II), suggesting the use of a Drucker-Prager type yield criterion.
- Eccentricity of the initial yield loci for aged IN718 defines the strength-differential effect that may be due to nonlinear elasticity (dislocation-precipitate interactions) and/or the effect of mean stress (increased dislocation density).
- Aged IN718 displays significantly more hardening behavior than solutioned IN718.
- Subsequent yield loci indicate anisotropic hardening that is predominantly kinematic and secondarily distortional. In addition, there may be a slight cross effect for solutioned IN718.

REFERENCES

Abdel-Kader, M.S., Eftis, J., and Jones, D.L. (1986), "Modeling the viscoplastic behavior of inconel 718 at 1200 °F," NASA CP–10010: Nonlinear Constitutive Relations for High Temperature Applications, pp. 37–68.

Battiste, R.L. and Ball, S.J. (1986), "Determination of surfaces of constant inelastic strain rate at elevated temperature," NASA CP–2444: Turbine Hot Section Technology, pp. 307–325.

Dieter, G.E. (1988), Mechanical Metallurgy. McGraw-Hill, London.

Drucker, D.C. (1973), "Plasticity theory, strength-differential (SD) phenomenon, and volume expansion in metals and plastics," Metall. Trans., Vol. 4, pp. 667–673.

Drucker, D.C. and Prager, W. (1952), "Soil mechanics and plastic analysis or limit design," Q. Appl. Math., Vol. 10, pp. 157.

Ellis, J.R. and Bartolotta, P.A. (1997), "Adjustable work coil fixture facilitating the use of induction Heating in mechanical testing," Multiaxial Fatigue and Deformation Testing Techniques, ASTM STP 1280, S. Kalluri and P.J. Bonacuse, Eds., American Society for Testing and Materials, pp. 43–62.

Fournier, D. and Pineau, A. (1977), "Low cycle fatigue behavior of inconel 718 at 298 K and 823 K," Metall. Trans., Vol. 8A, pp. 1095–1105.

Gil, C.M. (1998), "Determination of yield and flow surfaces for inconel 718 under axial-torsional loading at temperatures up to 649 °C," Masters thesis, Penn State University.

Gil, C.M., Lissenden, C.J., and Lerch, B.A. (1998a), "Rate-dependent flow surfaces for inconel 718," In preparation.

Gil, C.M., Lissenden, C.J., and Lerch, B.A. (1998b), "An investigation of anomalous behavior in metallic-based materials under compressive loading," NASA TM–206640, NASA Lewis Research Center, Cleveland, Ohio.

Hecker, S.S. (1973), "Influence of deformation history on the yield locus and stress-strain behavior of aluminum and copper," Metall. Trans., Vol. 4, no. 4, pp. 985–989.

Hecker, S.S. (1976), "Experimental studies of yield phenomena in biaxially loaded metals," Constitutive Equations in Viscoplasticity: Computational and Engineering Aspects, ASME, pp. 1–33.

Helling, D.E., Miller, A.K., and Stout, M.G. (1986), "An experimental investigation of the yield loci of 1100-0 aluminum, 70:30 brass, and an overaged 2024 aluminum alloy after various prestrains," J. Eng. Mater. Technol., Vol. 108, pp. 313–320.

Hirth, J.P. and Cohen, M. (1970), "On the strength-differential phenomenon in hardened steel," Metall. Trans., Vol. 1, pp. 3–8.

Kalish, D. and Cohen, M. (1969), "Anisotropy of properties in martensite as developed by thermomechanical treatments," Trans. ASM, Vol. 62, no. 2, pp. 353–361.

Kalluri, S. and Bonacuse, P.J. (1990), "A data aquisition and control program for axial-torsional fatigue testing," Applications of Automation Technology to Fatigue and Fracture Testing, ASTM STP 1092, A.A. Braun, N.E. Ashbaugh, and F.M. Smith, Eds., American Society for Testing and Materials, Philadelphia, pp. 269–287.

Kalluri, S., Rao, K.B.S., Halford, G.R., and McGaw, M.A. (1997), "Deformation mechanisms and fatigue behavior of prestrained inconel 718 superalloy," Proceedings of the Fourth International Special Emphasis Symposium on Superalloys 718, 625, 706 and Derivatives, Pittsburgh, PA, June 15–18.

Khan, A. and Wang, X. (1993), "An experimental study on subsequent yield surface after finite shear prestraining," Int. J. Plasticity, Vol. 9, pp. 889–905.

Khan, A. and Huang, S. (1995), Continuum Theory of Plasticity. John Wiley & Sons, New York.

Li, K. (1995), "Experimental evaluation of a viscoplastic constitutive model," AIAA/ASME/ASCE/AHS/ASC, Structures, Structural Dynamics and Materials Conference, 36th, New Orleans, LA, April 10–13.

Lissenden, C.J., Lerch, B.A., Ellis, J.R., and Robinson, D.N. (1997), "Experimental determination of yield and flow surfaces under axial-torsional loading," *Multiaxial Fatigue and Deformation Testing Techniques, ASTM STP 1280*, S. Kalluri and P.J. Bonacuse, Eds., American Society for Testing and Materials, pp. 92–112.

Michno, M.J., Jr. and Findley, W.N., (1974), "Subsequent yield surfaces for annealed mild steel under deadweight loading: aging, normality, convexity, corners, Bauschinger, and cross effects," J. Eng. Mater. Technol., Vol. 96, pp. 56–64.

Michno, M.J. and Findley, W.N. (1976), "An historical perspective of yield surface investigations for metals," Int. J. Nonlinear Mech., Vol. 11, pp. 59–82.

Nouailhas, D. and Cailletaud, G. (1996), "Finite element analysis of the mechanical behavior of two-phase single-crystal superalloys," Scripta Mat., Vol. 34, no. 4, pp. 565–571.

Oblak, J.M., Paulonis, D.F., and Duvall, D.S. (1974), "Coherency strengthening in Ni base alloys hardened by DO_{22} γ' precipitates," Metall. Trans., Vol. 5, pp. 143–153.

Phillips, A., Liu, C.S., and Justusson, J.W. (1972), "An experimental investigation of yield surfaces at elevated temperatures," Acta Mech., Vol. 14, pp. 119–146.

Phillips, A. and Lu, W. (1984), "An experimental investigation of yield surfaces and loading surfaces of pure aluminum with stress-controlled and strain-controlled paths of loading," J. Eng. Mater. Technol., Vol. 106, pp. 349–354.

Phillips, A. and Moon, H. (1977), "An experimental investigation concerning yield surfaces and loading surfaces," Acta Mech. Vol. 27, pp. 91–102.

Radcliffe, S.V. and Leslie, W.C. (1969), Reported at the 1969 Spring Meeting of TMS-AIME by G.C. Rauch and W.C. Leslie: J. Metals, vol. 21, no. 3, p. 27a.

Rauch, G.C., Daga, R.L., Radcliffe, S.V., Sober, R.J., and Leslie, W.C. (1975), "Volume expansion, pressure effects, and the strength differential in as-quenched iron-carbon martensite," Metall. Trans. A, Vol. 6A, no. 12, pp. 2279–2287.

Spitzig, W.A., Sober, R.J., and Richmond, O. (1975), "Pressure dependence of yielding and associated volume expansion in tempered martensite," Acta Metall., Vol. 23, pp. 885–893.

Stouffer, D.C. and Dame, L.T. (1996), Inelastic Deformation of Metals: Models, Mechanical Properties, and Metallurgy, John Wiley & Sons, Inc., New York, pp. 36–40.

Sundararaman, M., Mukhopadhyay, P., and Banerjee, S. (1988), "Deformation behavior of γ' strengthened inconel 718," Acta Metall., Vol. 36, No. 4, pp. 847–864.

Williams, J.F. and Svensson, N.L. (1970), "Effect of torsional prestrain on the yield locus of 110-F aluminum," J. Strain Analysis, Vol. 6, pp. 263–272.

Winstone, M.R. (1984), "Influence of prestress on the yield surface of the cast nickel superalloy MAR-M002 at elevated temperature," Proceedings of the 4th International Conference, Vol. 1, Stockholm, Swen Pergamon Press Oxford, England, pp. 199–205.

Worthem, D.W., Altstetter, C.J., Robertson, I.M., and Socie, D.F. (1989), "Cyclic deformation and damage structure in inconel 718," Biaxial and Multiaxial Fatigue, EGF 3 (Edited by M. W. Brown and K. J. Miller), Mechanical Engineering Publications, London, pp. 131–143.

Wu, Han C. and Yeh, Wei C. (1991), "On the experimental determination of yield surfaces and some results of annealed 304 stainless steel," Int. J. Plasticity, Vol. 7, pp. 803–826.

TABLE I.—MATERIAL COMPOSITION OF INCONEL 718

Element	Content, wt.%
Ni	53.58
Cr	17.52
Mo	2.87
(Nb+Ta)	5.19
Ti	0.95
Al	0.57
Co	0.39
C	0.034
S	0.002
Mn	0.120
Si	0.070
B	0.004
Cu	0.050
P	0.006
Fe	Bal.

TABLE II.— RADIUS AND CENTER OF EACH INITIAL YIELD LOCUS FOR SOLUTIONED AND AGED IN718 AS A FUNCTION OF TEMPERATURE

	Solutioned			Aged		
Temperature, °C	Radius of Mises circle, MPa	Center of Mises circle, MPa	Strength-differential, percent	Radius of Mises circle, MPa	Center of Mises circle, MPa	Strength-differential, percent
23	248	(0.0, 0.0)	0	655	(–138.0, 0.0)	42
371	207	(13.8,0.0)	13	– –	– – – – – –	– –
454	193	(–27.5, 0.0)	28	– –	– – – – – –	– –
649	– –	– – – – – –	– –	448	(–145.0, 0.0)	65

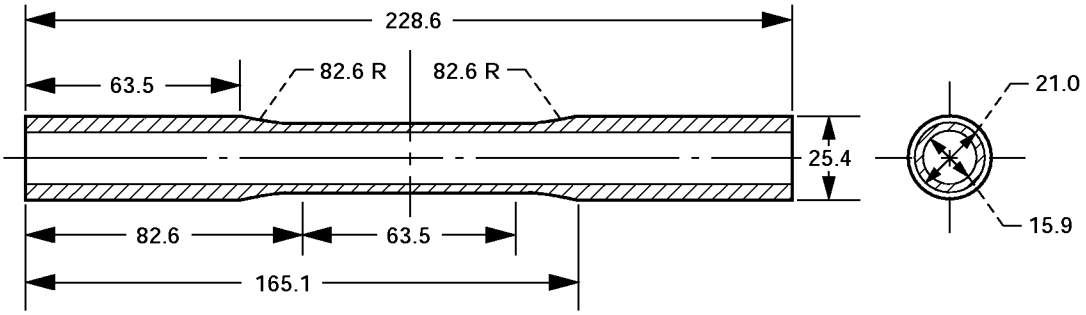

Figure 1.—Typical specimen geometry (all dimensions are in millimeters).

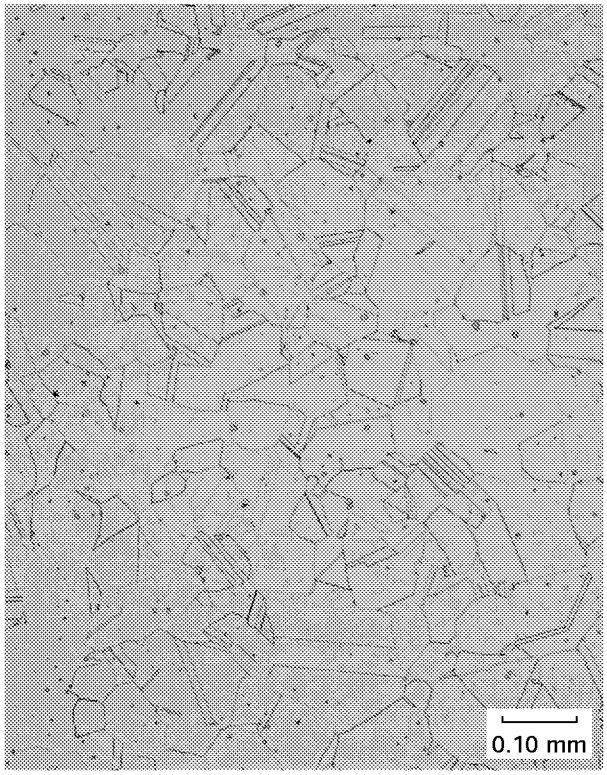

Figure 2.—Microstructure of solutioned Inconel 718 (optical microscopy). The microstructure for aged Inconel 718 was similar.

Figure 3.—Transmission electron microscopy of aged Inconel 718 showing γ" precipitation.

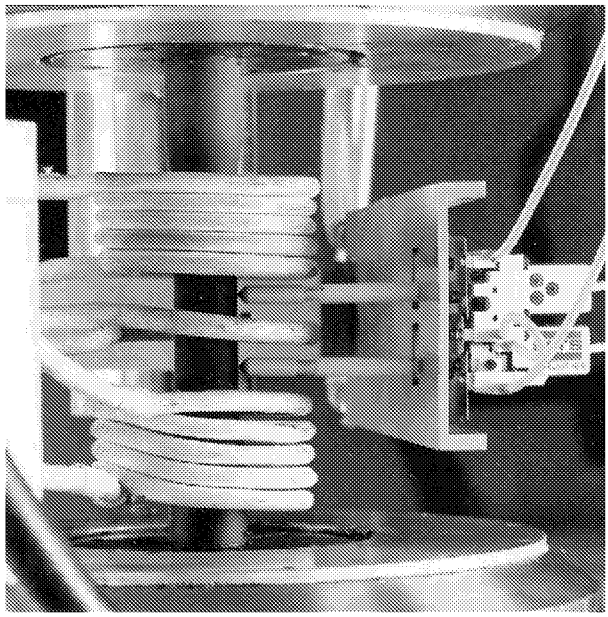

Figure 4.—Close-up of specimen, extensometer, and heating coils.

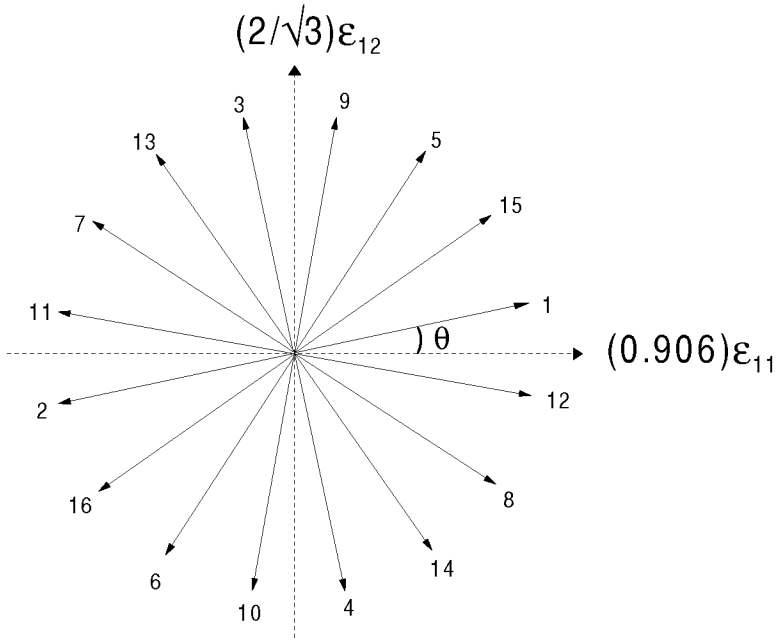

Probe Number	Probe Angle	Probe Number	Probe Angle
1	12°	9	79°
2	192°	10	259°
3	102°	11	170°
4	282°	12	350°
5	57°	13	125°
6	237°	14	305°
7	147°	15	35°
8	327°	16	215°

Figure 5.—Probe directions used in determining a yield locus.

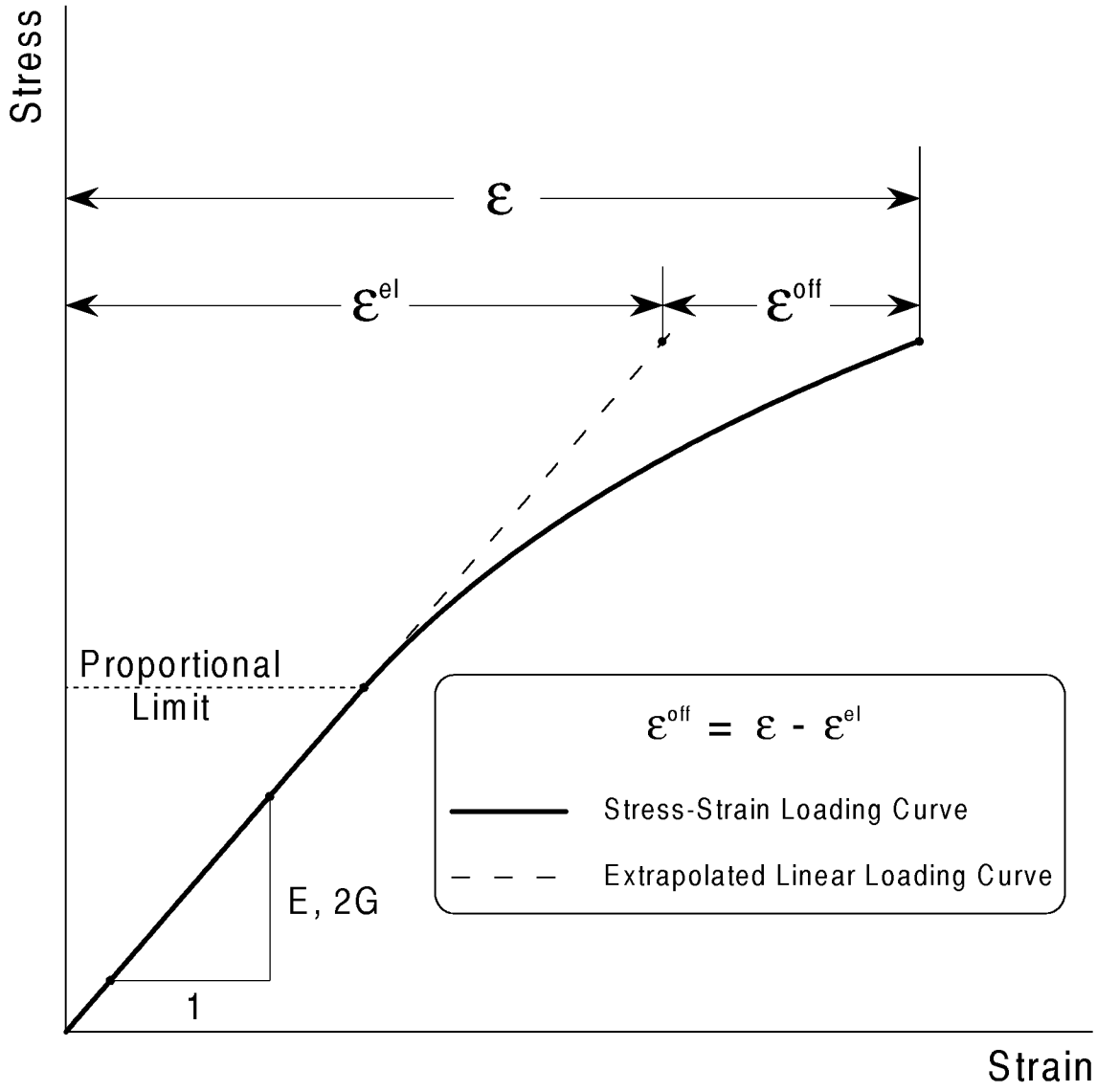

Figure 6.—Calculation of E, G, and ε^{off} during experiments.

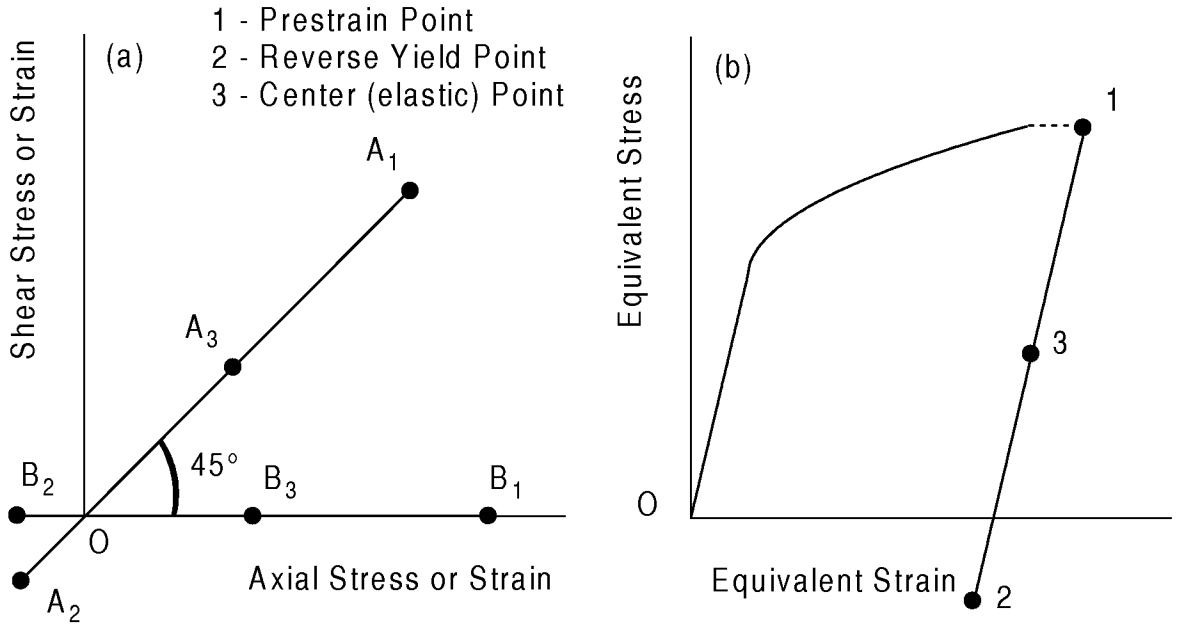

Figure 7.—Prestrain paths shown (a) in the stress or strain plane, and (b) as the equivalent stress-strain response.

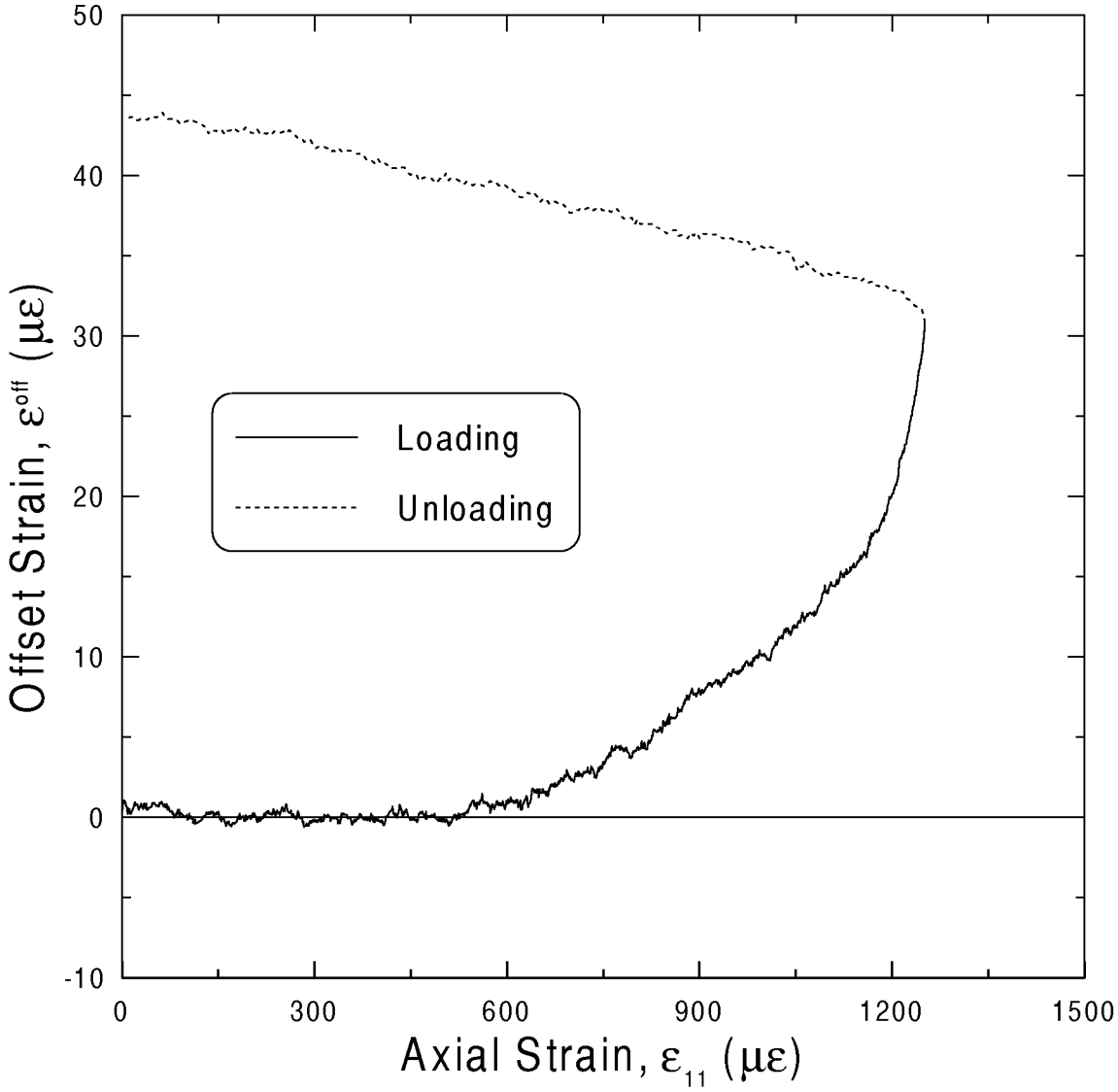

Figure 8.—Offset strain versus strain during tensile loading for solutioned IN718.

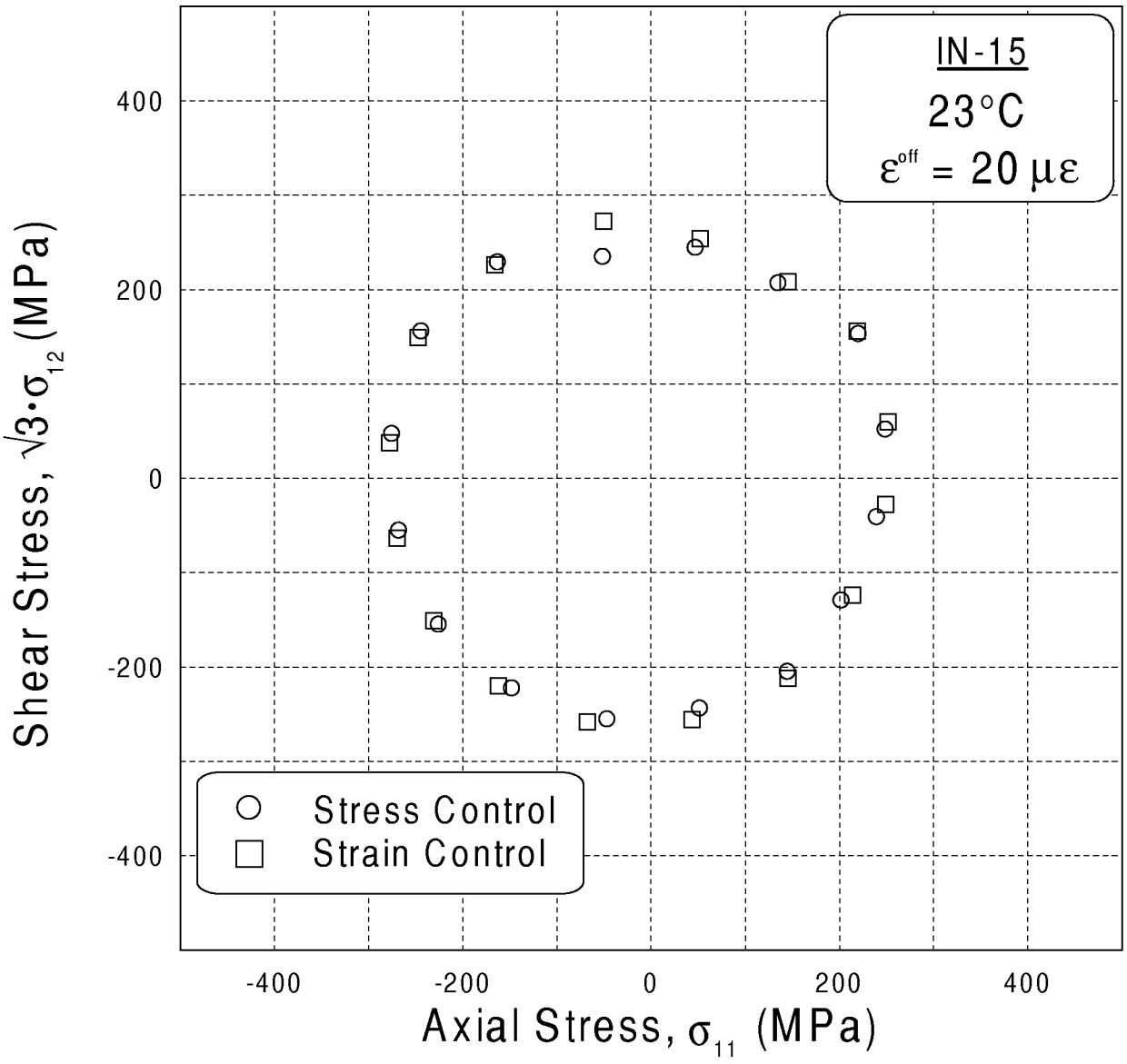

Figure 9.—Yield loci for solutioned, non-pristine IN718 determined under stress and strain control at room temperature.

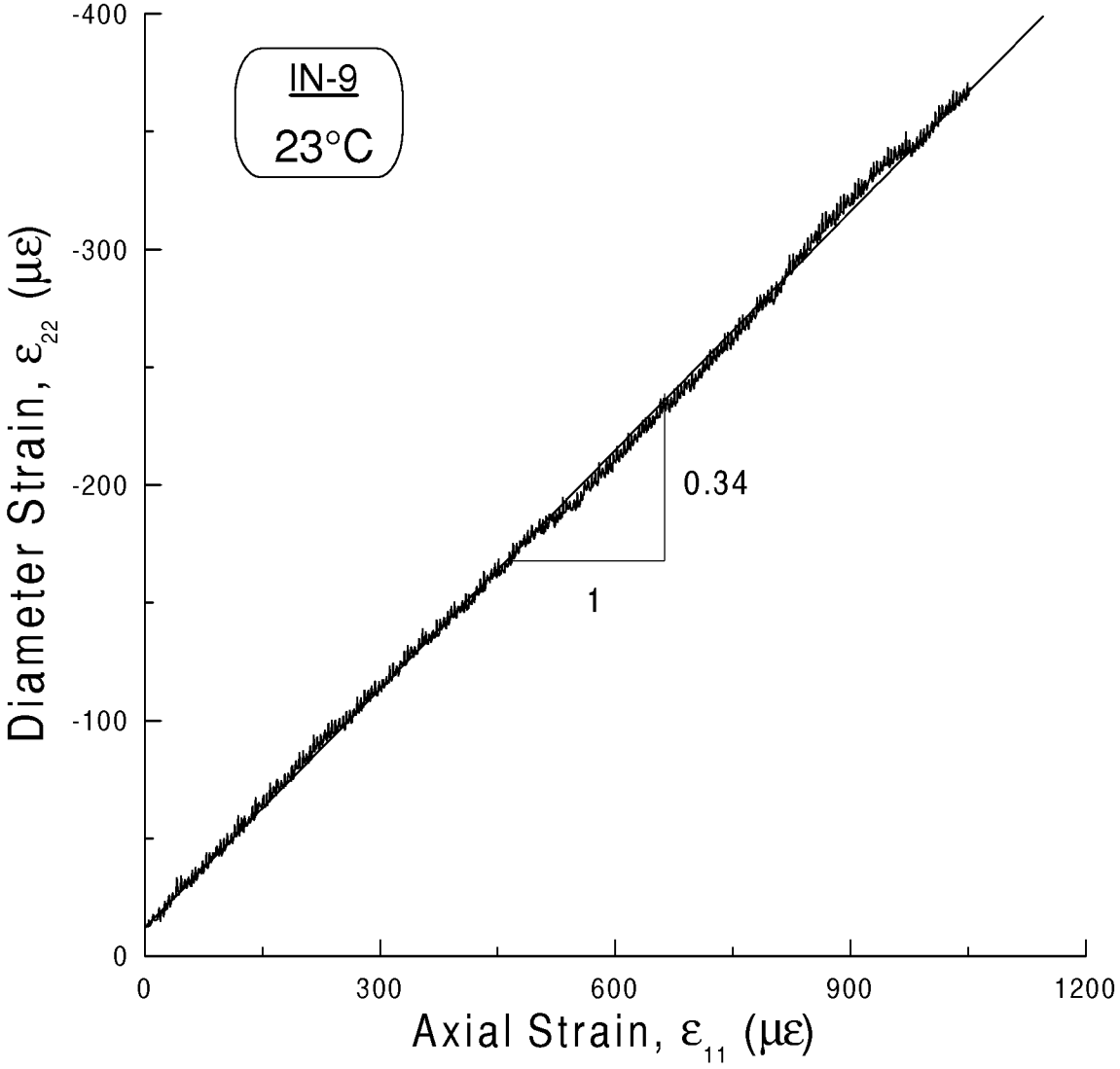

Figure 10.—The slope of the diametral strain versus axial strain gives a Poisson's ratio of 0.34.

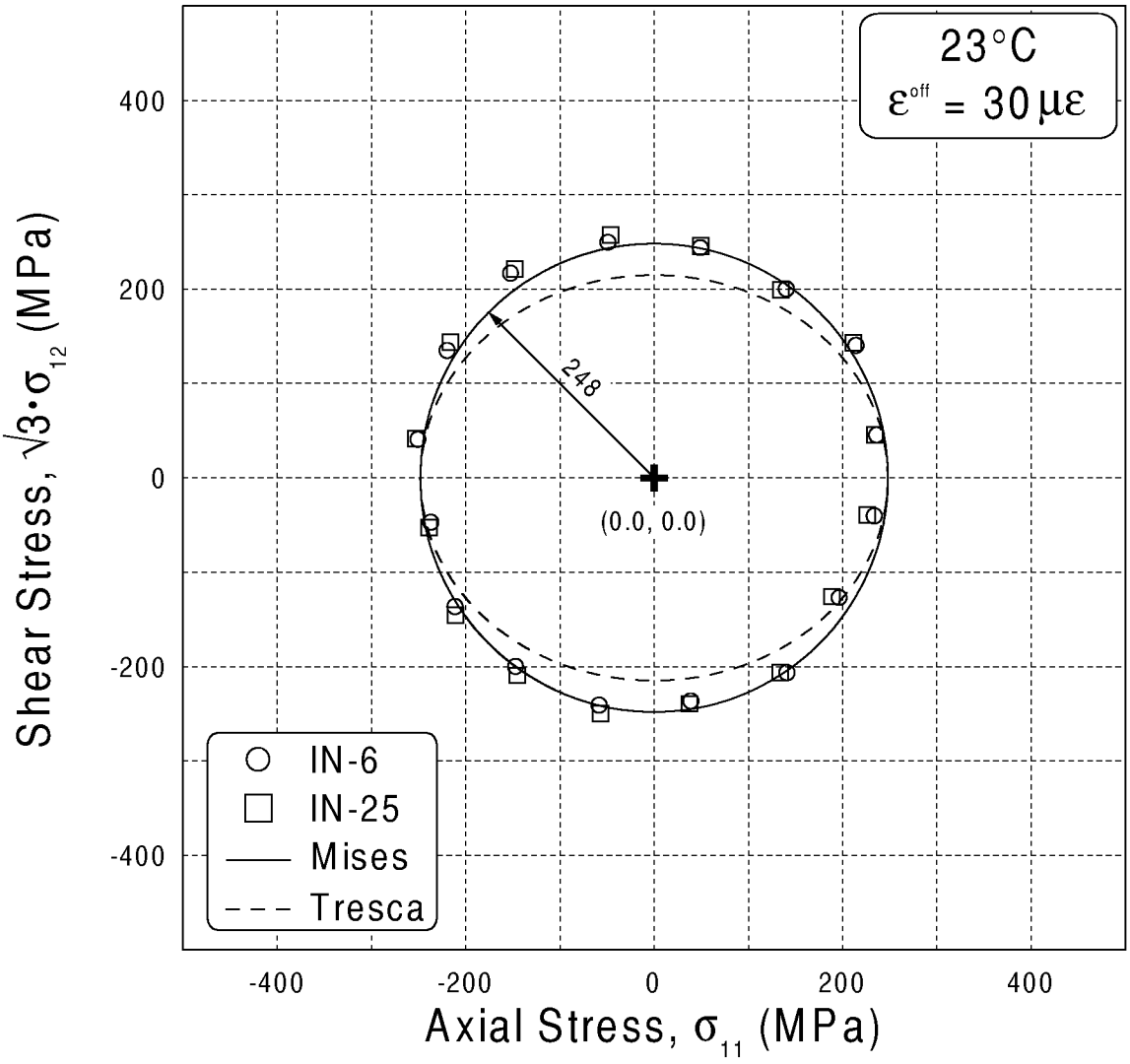

Figure 11.—Initial yield loci for solutioned IN718 at room temperature. The von Mises and Tresca yield criteria are also shown.

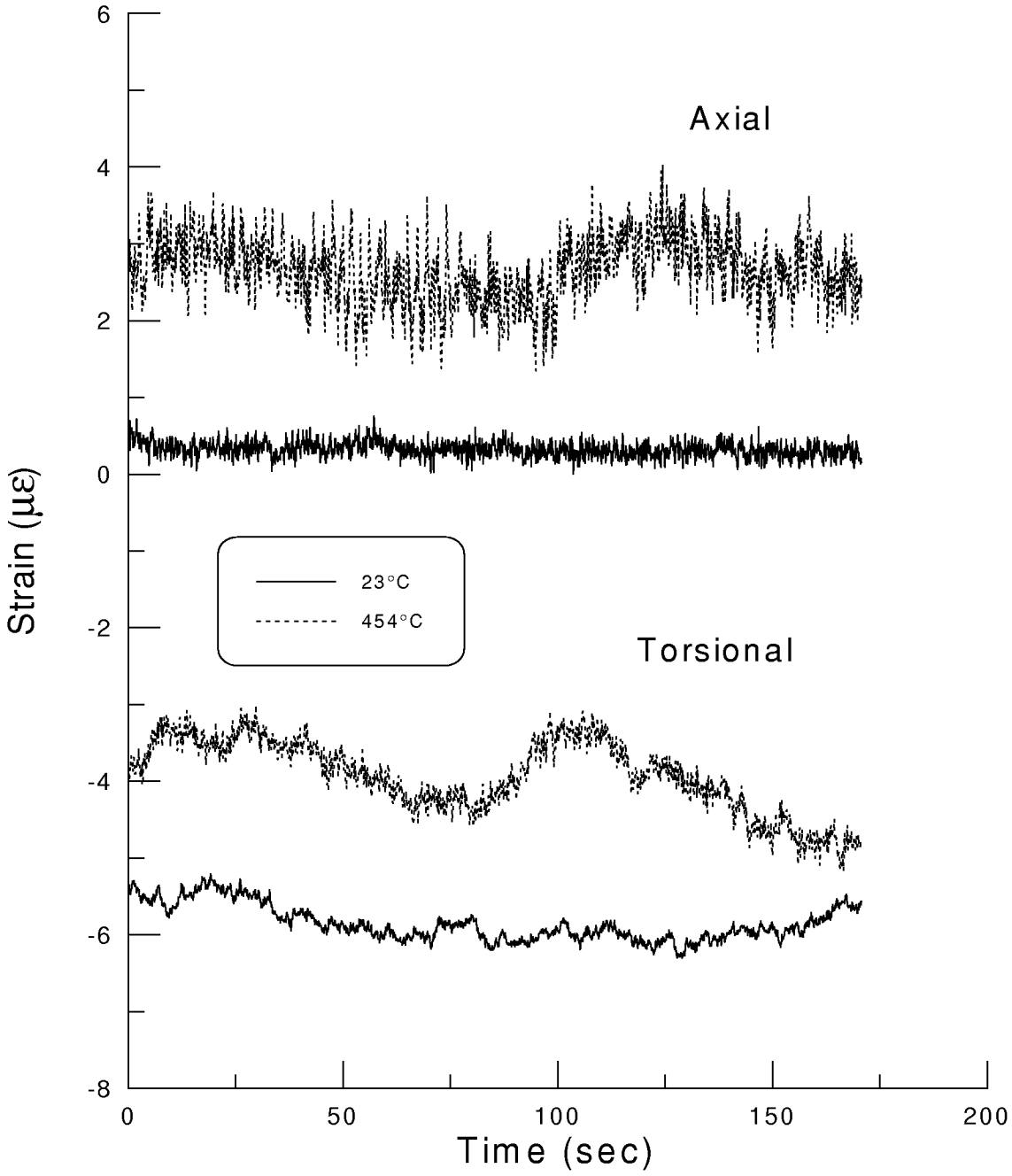

Figure 12.—Comparison of heater noise at 23 and 454 °C.

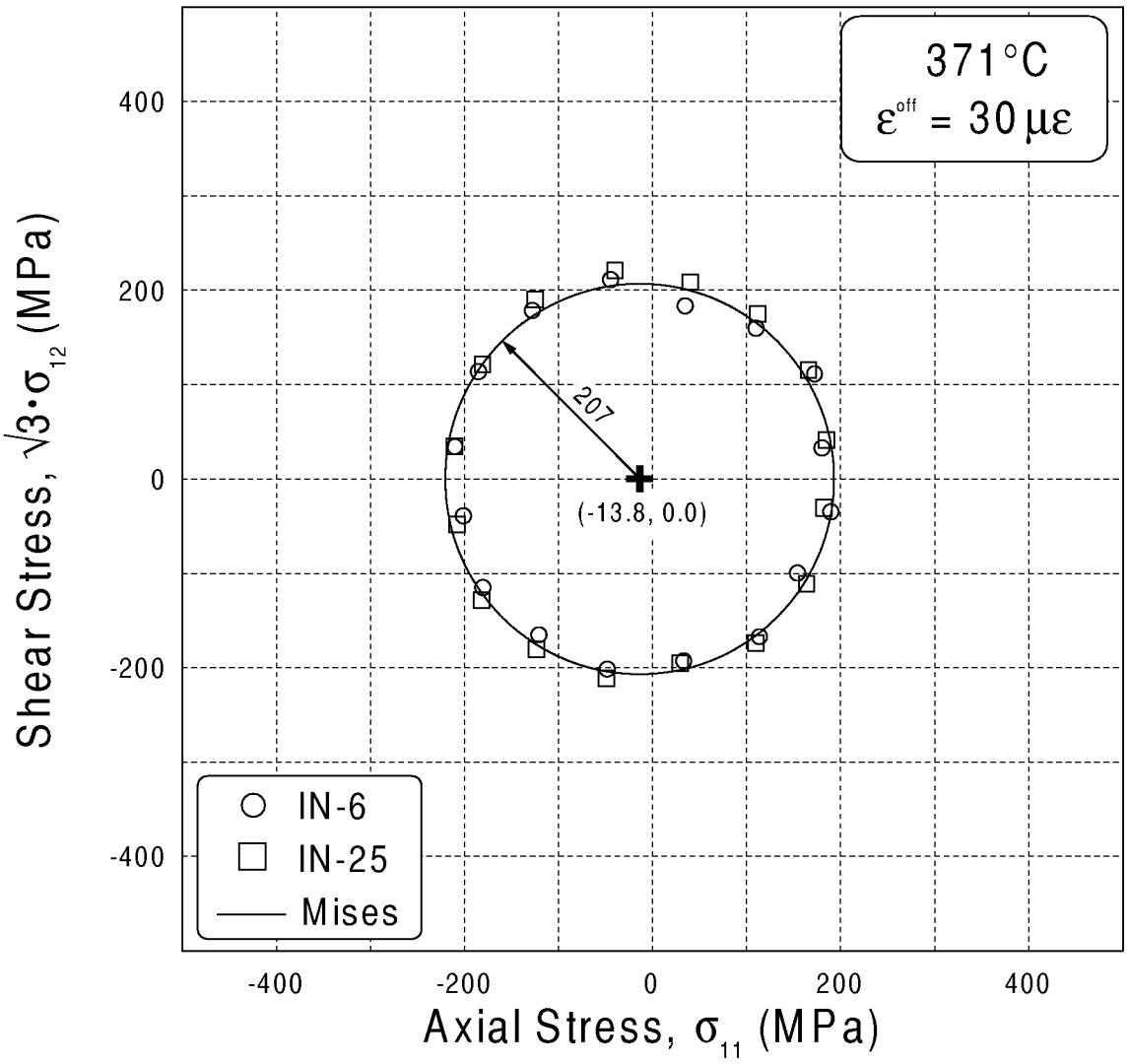

Figure 13.—Initial yield loci for solutioned IN718 at 371 °C.

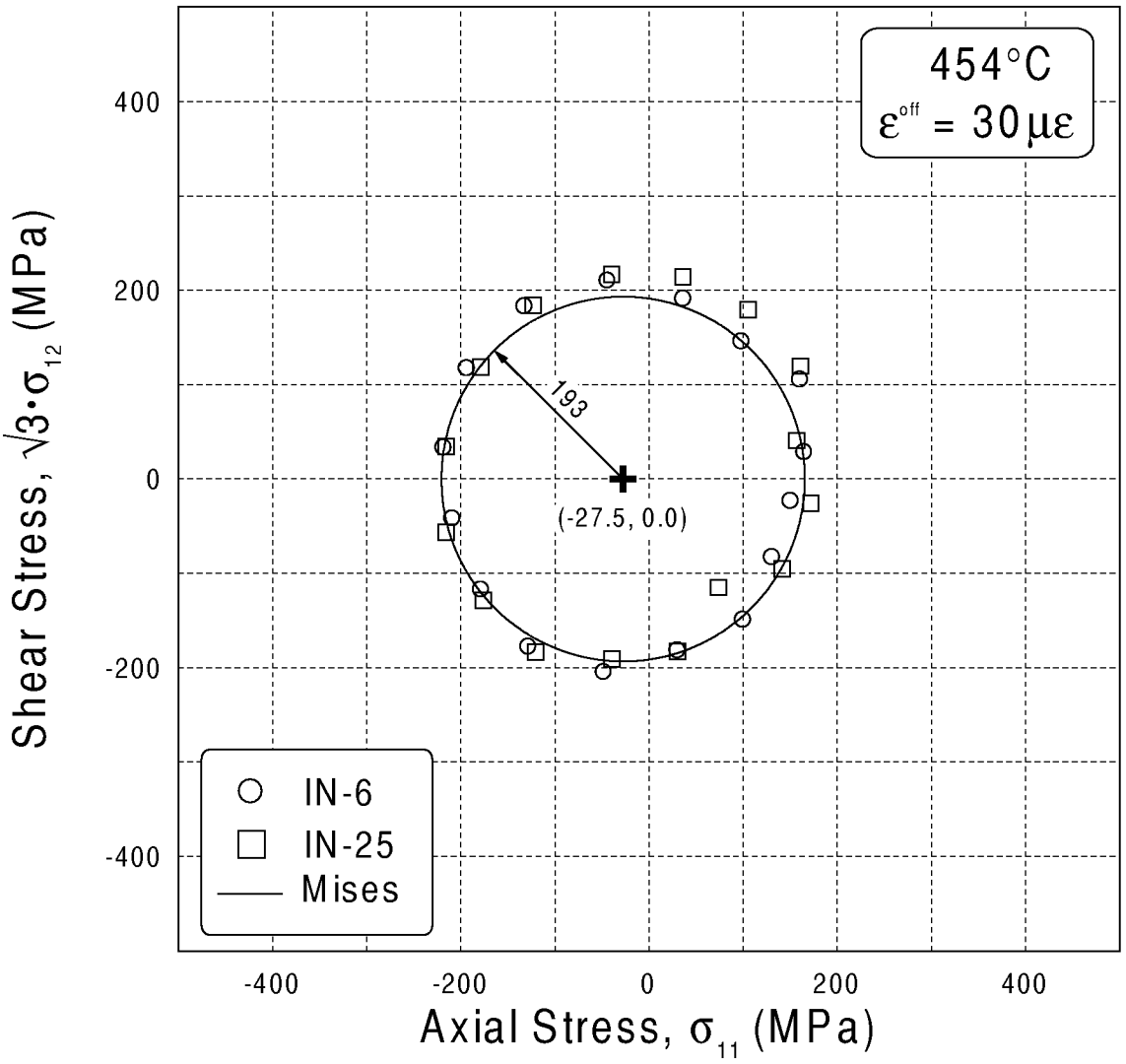

Figure 14.—Initial yield loci for solutioned IN718 at 454 °C.

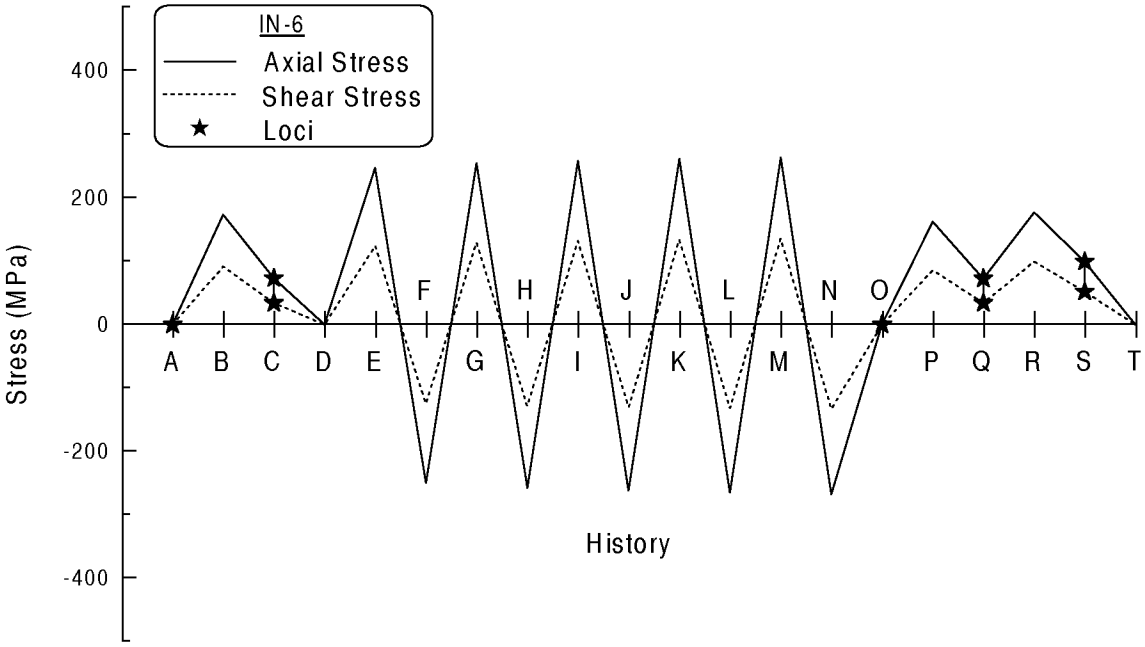

Figure 15.—Loading history for specimen IN-6 indicating where yield loci were determined.

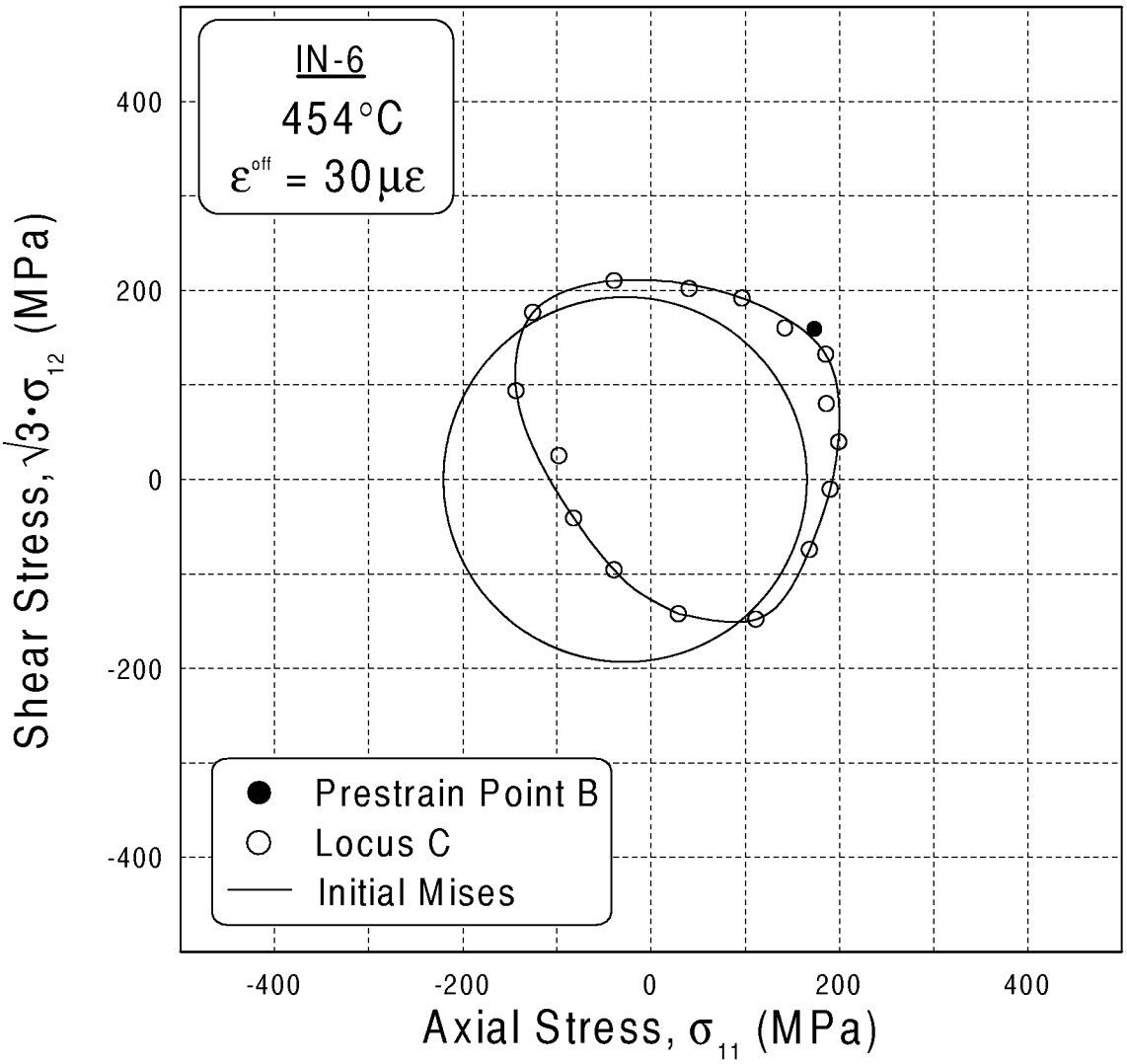

Figure 16.—Yield locus subsequent to a tension-torsion prestrain of 500 με offset for solutioned IN718 at 454 °C.

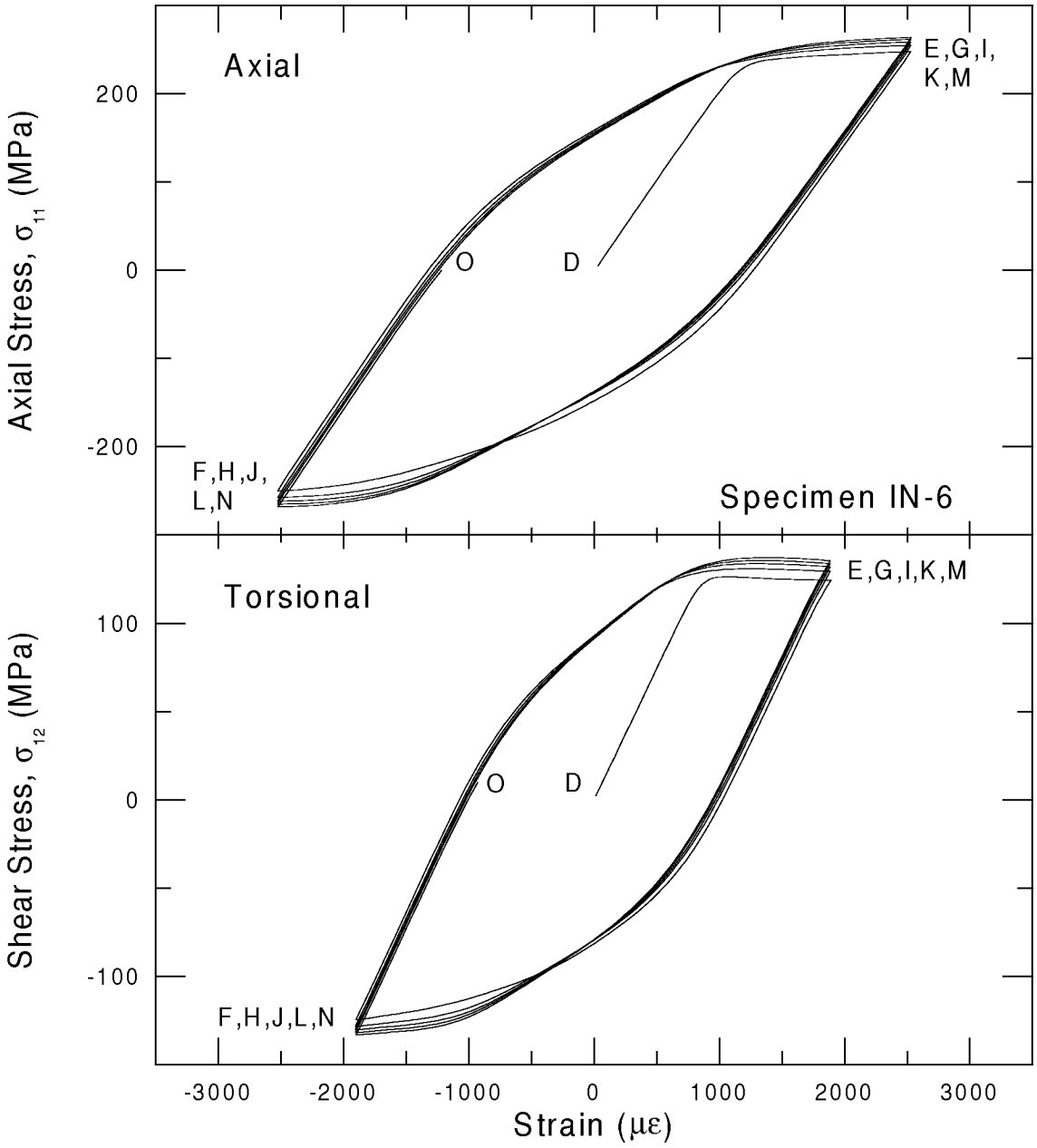

Figure 17.—Combined axial-torsional cyclic loading at room temperature ($\theta = 45°$). Five complete cycles beginning and ending at zero stress.

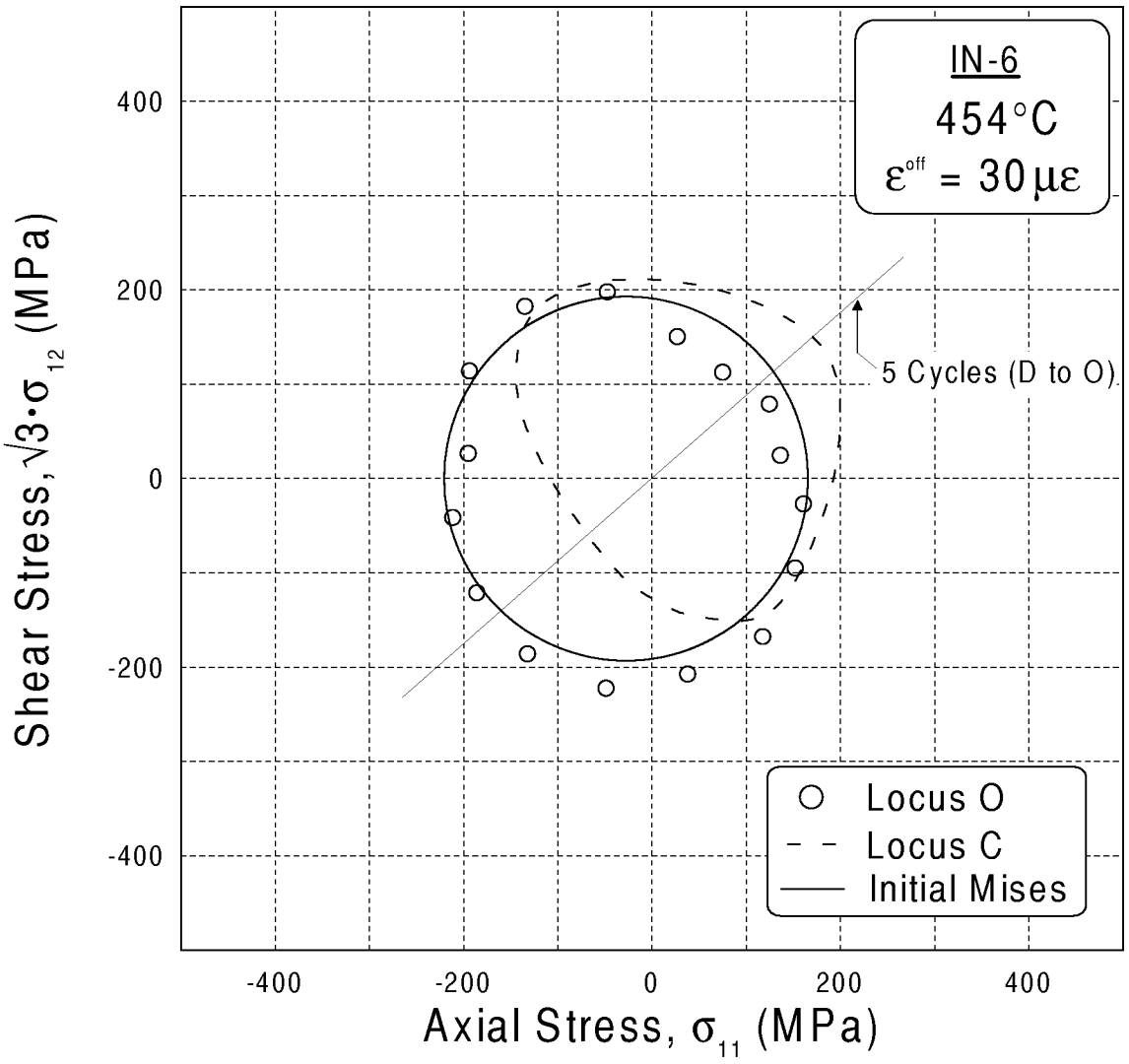

Figure 18.—Yield locus subsequent to cyclic loading for solutioned IN718 at 454 °C.

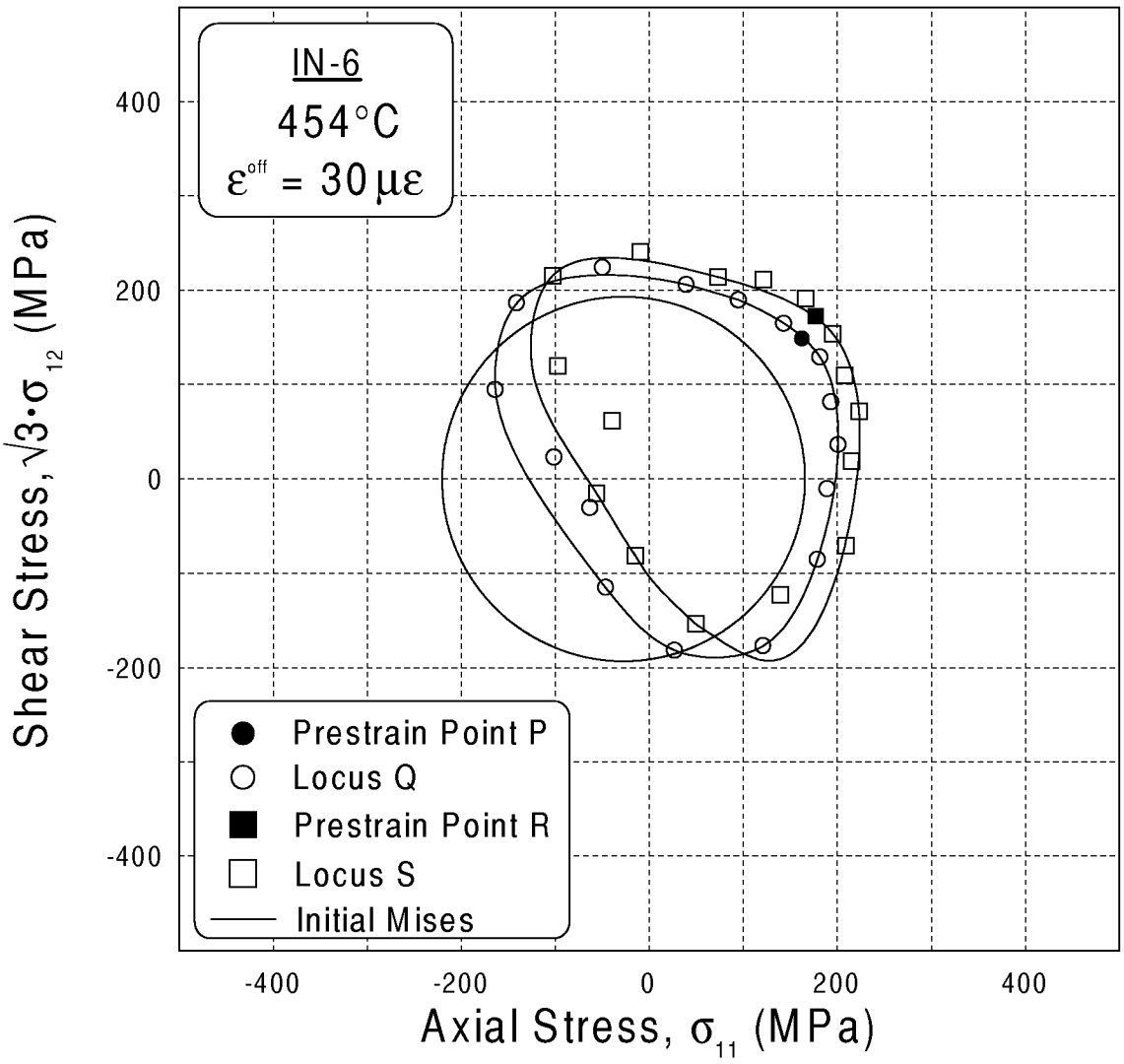

Figure 19.—Subsequent yield loci for proportional prestraining to 1000 με offset (locus Q) and 1500 (locus Q) and 1500 (locus Q) and 1500 με offset (locus S) for solutioned IN718 at 454 °C.

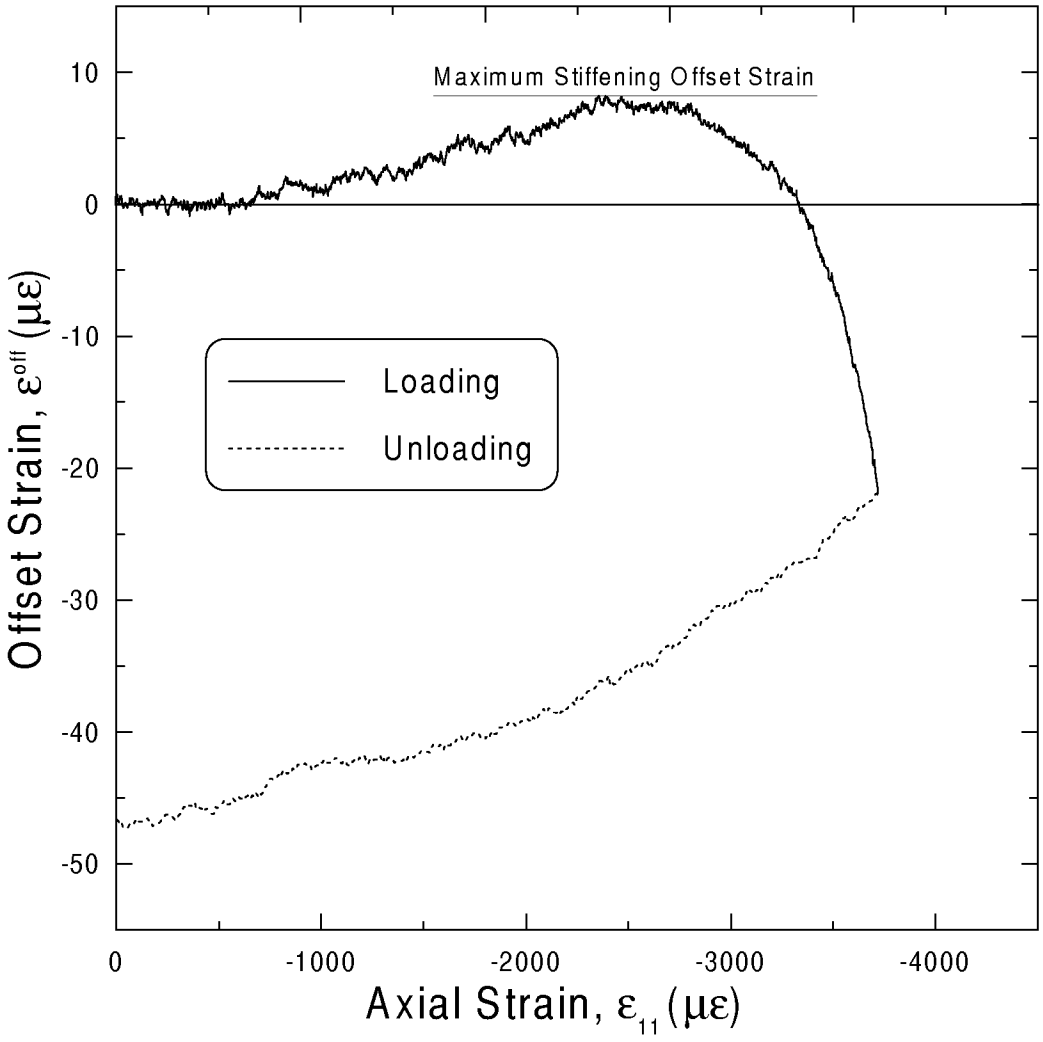

Figure 20.—Offset strain versus strain during compressive loading for aged IN718, indicating stiffening.

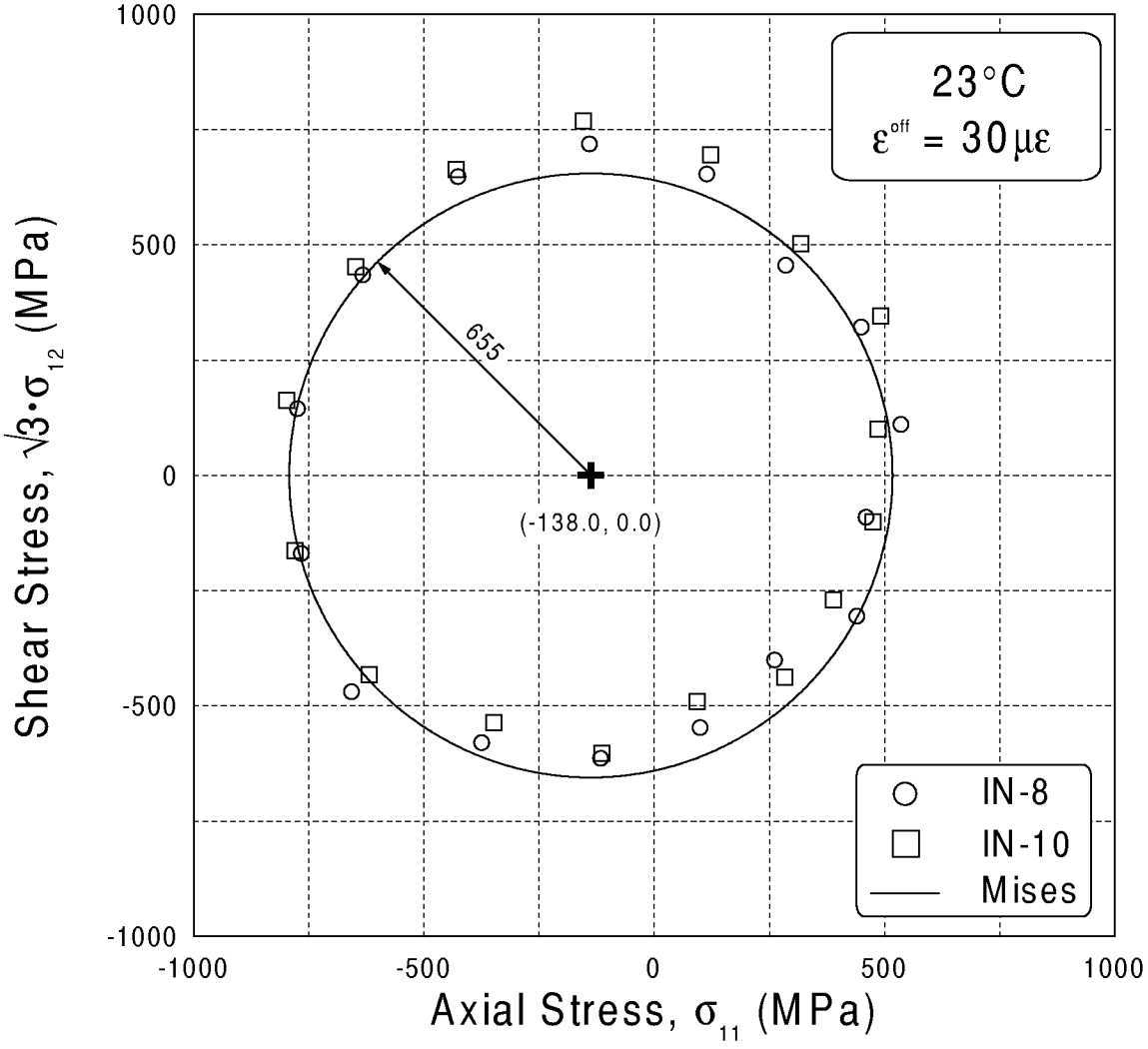

Figure 21.—Initial yield loci for aged IN718 at room temperature. An eccentric von Mises circle is also shown.

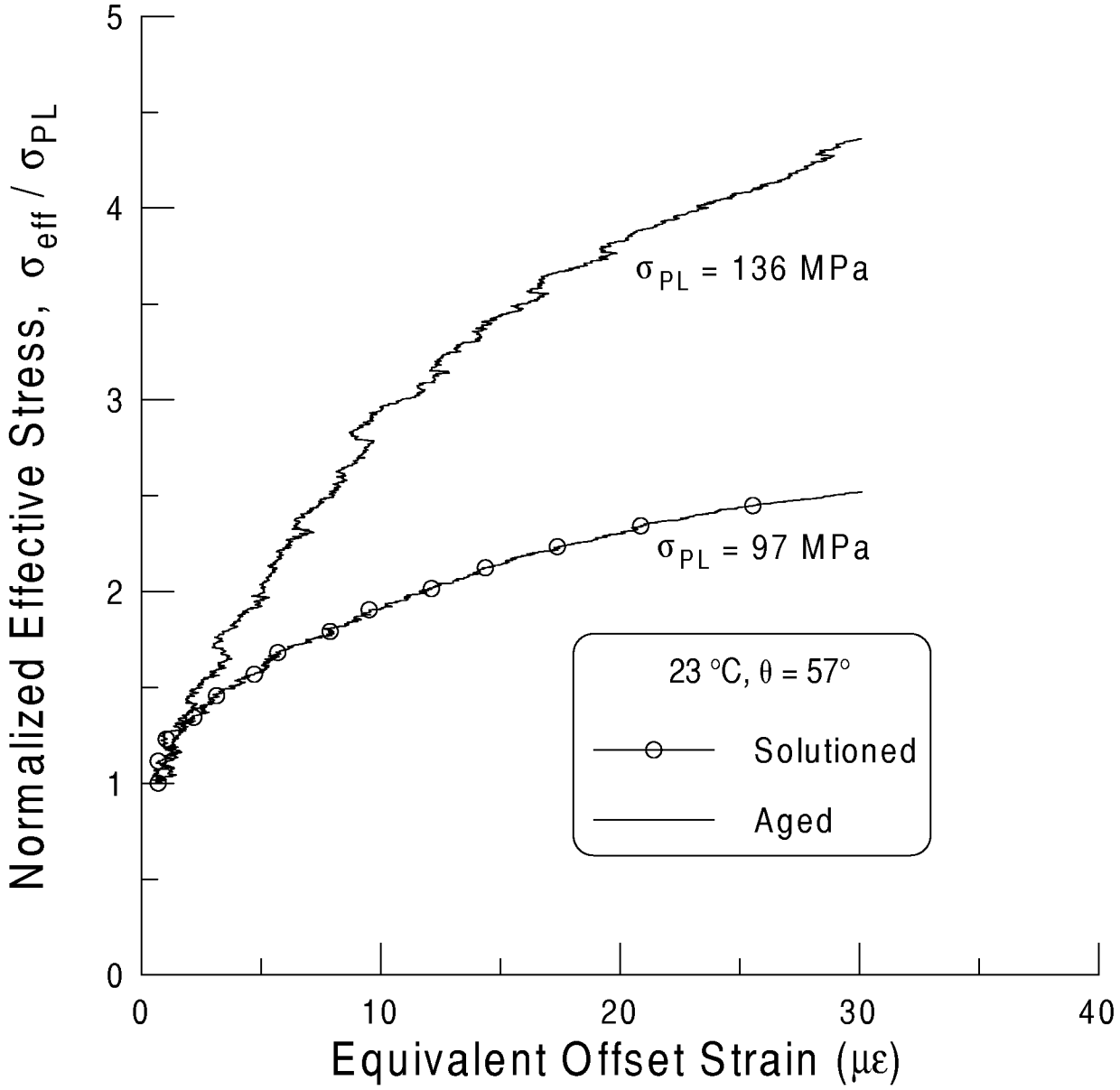

Figure 22.—Stress versus offset strain for solutioned and aged IN718 under tension and torsion.

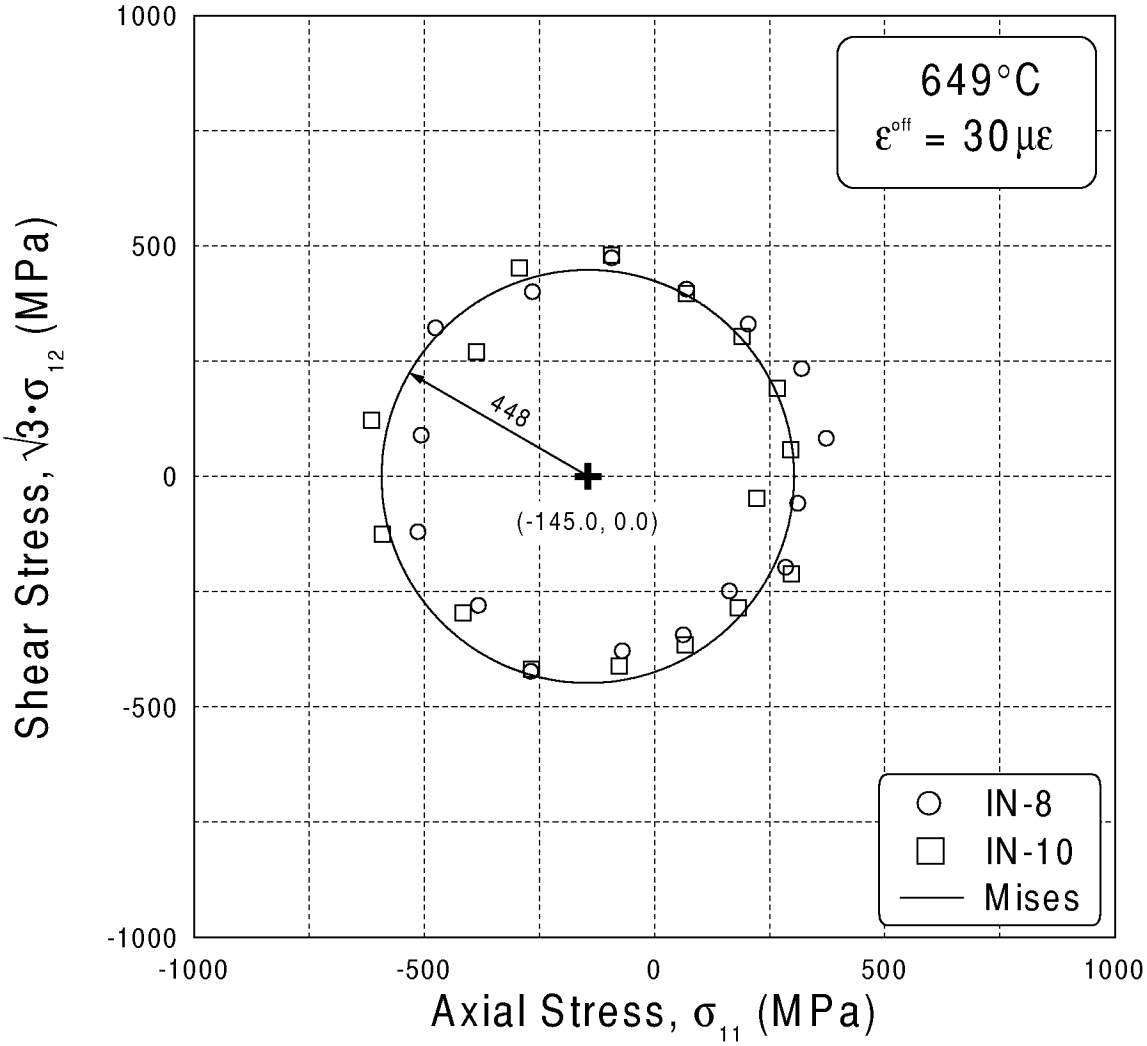

Figure 23.—Initial yield loci for aged IN718 at 649 °C.

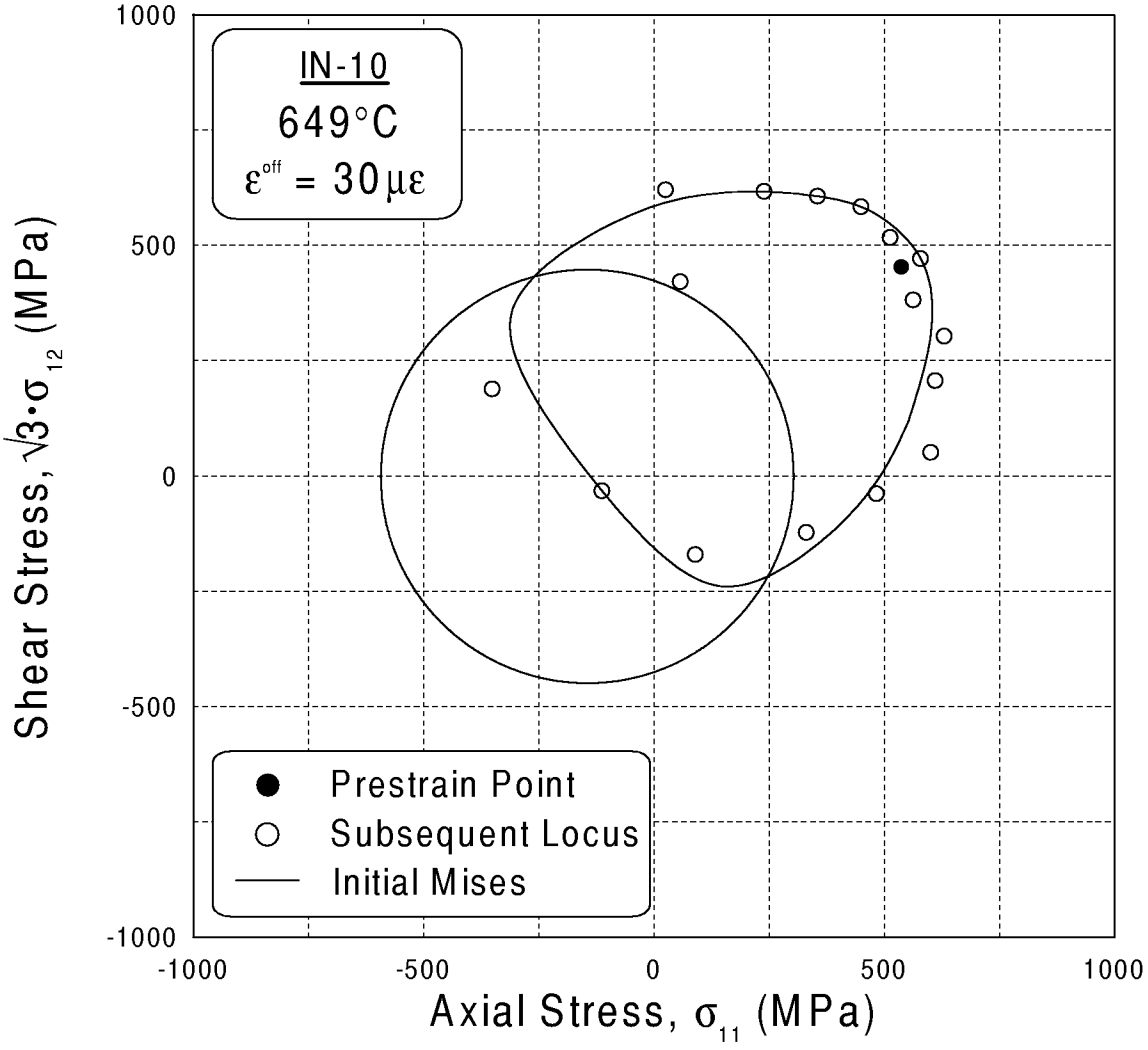

Figure 24.—Yield locus subsequent to a tension-torsion prestrain of 500 με offset for aged IN718 at 649 °C.

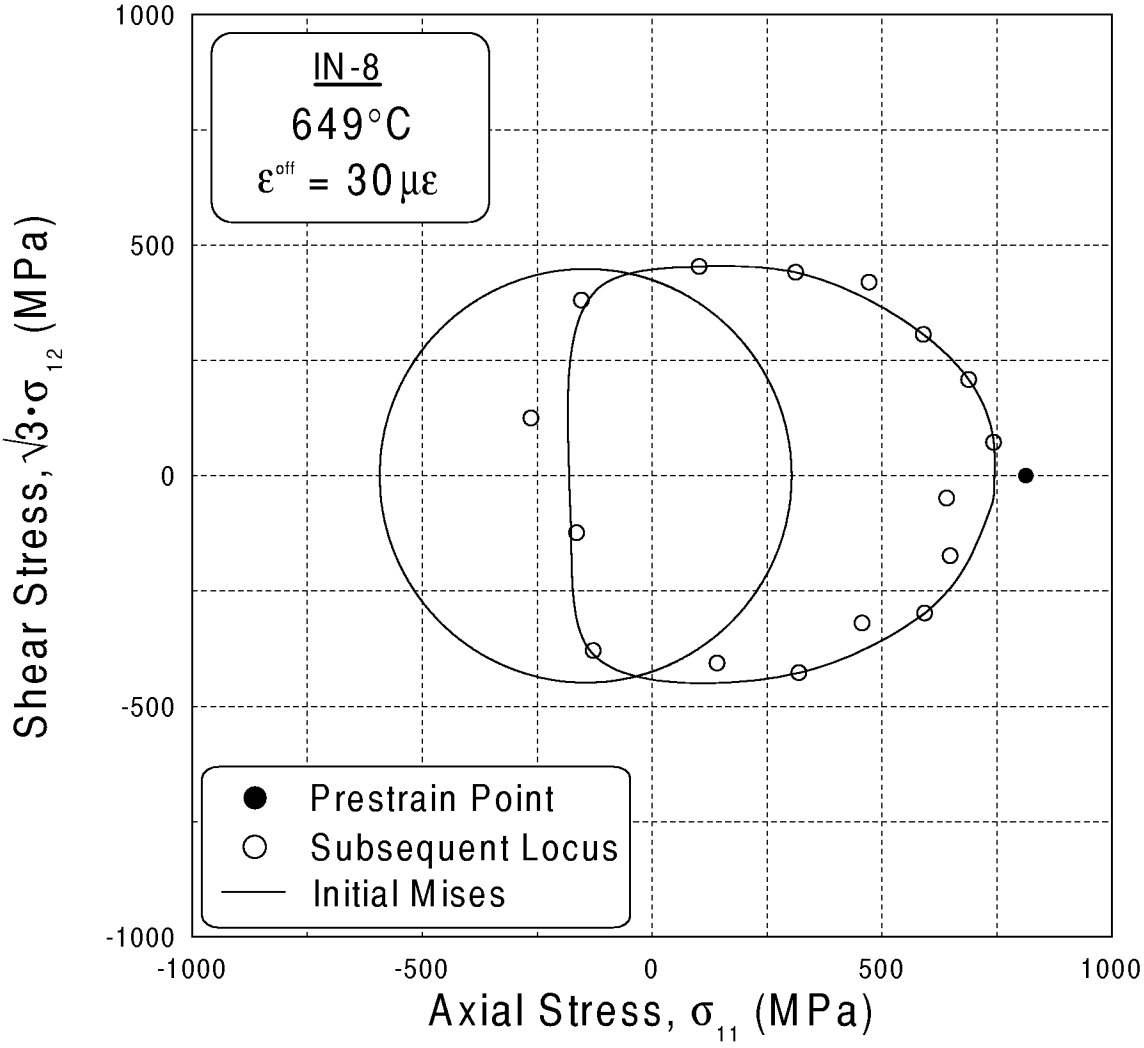

Figure 25.—Yield locus subsequent to a tension prestrain of 9000 με (0.9%) for aged IN718 at 649 °C.

REPORT DOCUMENTATION PAGE

Form Approved
OMB No. 0704-0188

1. AGENCY USE ONLY (*Leave blank*)	2. REPORT DATE	3. REPORT TYPE AND DATES COVERED
	November 1998	Technical Memorandum

4. TITLE AND SUBTITLE

Determination of Yield in Inconel 718 for Axial-Torsional Loading at Temperatures up to 649 °C

5. FUNDING NUMBERS

WU–523–21–13–00

6. AUTHOR(S)

Christopher M. Gil, Cliff J. Lissenden, and Bradley A. Lerch

7. PERFORMING ORGANIZATION NAME(S) AND ADDRESS(ES)

National Aeronautics and Space Administration
Lewis Research Center
Cleveland, Ohio 44135–3191

8. PERFORMING ORGANIZATION REPORT NUMBER

E–11380

9. SPONSORING/MONITORING AGENCY NAME(S) AND ADDRESS(ES)

National Aeronautics and Space Administration
Washington, DC 20546–0001

10. SPONSORING/MONITORING AGENCY REPORT NUMBER

NASA TM—1998-208658

11. SUPPLEMENTARY NOTES

Christopher M. Gil and Cliff J. Lissenden, Pennsylvania State University, University Park, Pennsylvania 16802–1009. Responsible person, Bradley A. Lerch, organization code 5920, (216) 433–5522.

12a. DISTRIBUTION/AVAILABILITY STATEMENT

Unclassified - Unlimited
Subject Categories: 26 and 39 Distribution: Nonstandard

This publication is available from the NASA Center for AeroSpace Information, (301) 621–0390.

12b. DISTRIBUTION CODE

13. ABSTRACT ***(Maximum 200 words)***

An experimental program has been implemented to determine small offset yield loci under axial-torsional loading at elevated temperatures. The nickel-base superalloy Inconel 718 (IN718) was chosen for study due to its common use in aeropropulsion applications. Initial and subsequent yield loci were determined for solutioned IN718 at 23, 371, and 454°C and for aged (precipitation hardened) IN718 at 23 and 649°C. The shape of the initial yield loci for solutioned and aged IN718 agreed well with the von Mises prediction. However, in general, the centers of initial yield loci were eccentric to the origin due to a strength-differential (S-D) effect that increased with temperature. Subsequent yield loci exhibited anisotropic hardening in the form of translation and distortion of the locus. This work shows that it is possible to determine yield surfaces for metallic materials at temperatures up to at least 649°C using multiple probes of a single specimen. The experimental data is first-of-its-kind for a superalloy at these very high temperatures and will facilitate a better understanding of multiaxial material response, eventually leading to improved design tools for engine designers.

14. SUBJECT TERMS	15. NUMBER OF PAGES
Nickel alloy; Plasticity; Yield surface; Multiaxial loads	39
	16. PRICE CODE: A03

17. SECURITY CLASSIFICATION OF REPORT	18. SECURITY CLASSIFICATION OF THIS PAGE	19. SECURITY CLASSIFICATION OF ABSTRACT	20. LIMITATION OF ABSTRACT
Unclassified	Unclassified	Unclassified	